



**University of
Nottingham**

UK | CHINA | MALAYSIA

**Ionic Liquids as Potential Lubricants and Thermal Fluids
in Electric Vehicles**

Kent M. Stavenuiter

Thesis submitted to the University of Nottingham for the degree of
Master of Research

April 2024

Table of Contents

1. Abbreviations Table	3
2. Abstract	4
3. Introduction	5
4. Electric Vehicles	6
4.1. Electric Motor Challenges	6
4.1.1 Thermal Management of E-motors	7
4.1.2. Tribological Demands of Wet E-motors	8
5. Ionic Liquids	9
5.1 Cationic Structures	10
5.1.1 Aprotic Monocations	10
5.1.2 Protic Monocations	10
5.2.3 Dicationic ILs	11
5.2.4 Poly-ILs	12
5.2. Anion Selection	12
5.3. Anti-Wear and Friction Reduction Properties of ILs	12
6. Experimental	15
6.1 Synthesis and Characterisation	15
6.2 Analysis	21
7. Results and Discussion	23
7.1. DSC Analysis of Neat ILs	24
7.2. Thermal Stability of Neat ILs	30
7.3. Heat Capacity (C_p) of Neat ILs	33
7.4. Viscosity (μ, ν) and Density (ρ) of Neat ILs	35
7.5. ILs as EV fluid additives	38
7.5.1. Miscibility	38
7.5.2. Viscosity (μ, ν) and Density (ρ)	40
7.5.3. Viscosity Index, VI	44
7.5.4. Thermal Stability	46
8. Conclusion	49
9. Bibliography	51
10. Appendix	57

1. Abbreviations Table

ATF	Automatic transmission fluid
BEV	Battery electric vehicle
DIL	Dicationic ionic liquid
DSC	Differential Scanning Calorimetry
EV	Electric Vehicle
GHG	Greenhouse gas
HEV	Hybrid electric vehicle
ICE	Internal combustion engine
IL	Ionic liquid
PAO	poly-alpha-olefins
PIL	Protic ionic liquid
Poly-ILs	Ionic liquid polymers
RE-PM	Rare-earth permanent magnets
VI	Viscosity index
ZDDP	Zinc dithiophosphate

2. Abstract

With road transport accounting for a large percentage of greenhouse gas emissions (>25% in the UK), electric vehicles (EVs) have become an inevitable solution in combating rising global temperatures.¹ However, as EVs continue to develop, motor speeds are increasing significantly, as well as the temperatures of mechanical and electrical components. This has led to the need for new classes of vehicle fluids to provide high-performance lubrication in conjunction with thermal management. In this thesis, a range of ionic liquids, including the novel geminal dications $[C_{10}(C_1\text{Pyrr})_2][\text{NTf}_2]_2$ and $[\text{m-xyl}-(C_8\text{Im})_2][\text{NTf}_2]_2$, have been synthesised and thermophysical measurements have been collected to assess suitability as neat and additive bespoke fluids. $[P_{66614}][\text{DEHP}]$ and $[N_{888H}][\text{DEHP}]$ are shown to be effective additive species in a range of PAO base oils, providing improvements to the bulk physical properties at low %wt concentrations, in addition to the anti-wear improvements assessed in previous studies. It can be concluded that with additional material compatibility tests, ILs have potential to be highly effective as lubricants and thermal fluids in advanced EVs.

3. Introduction

In the wake of the climate crisis, nations are undergoing a rapid shift towards the electrification of greenhouse gas (GHG) emitting infrastructure in an attempt to prevent average global temperatures from reaching a 1.5 °C increase from preindustrial levels – as determined in the 2015 Paris Agreement.² The transport sector is a significant contributor to the current GHG levels in the atmosphere - in 2019, domestic transport was the UK's highest contributor, responsible for 27% of total emissions.¹ Within the EU-27, road transport accounted for the overwhelming majority of emissions in this sector (71.7%), notably larger than the emissions from civic aviation (13.4%).³ In response, nations are adopting electric vehicle (EV) technologies as a vital solution in reducing their emissions, leading to sales of EVs increasing substantially over the last decade – representing 11.6% of new EU registrations in 2020.³ In 2022 the UK set a target to end the sale of new diesel and petrol vehicles by 2030.⁴ Therefore, in the near future, it is very likely that EVs will become the dominant class of vehicles on our roads.

In order to improve the efficiency of EVs and to assist further integration into the road transport sector, solutions must be found for numerous vehicle design challenges. This includes reducing dependence on environmentally and economically costly rare-earth permanent magnets (RE-PMs), improving battery efficiency and range, and designing new lubricants and thermal fluids to facilitate the requirements of the new EV technologies.^{5,6,7}

Over the past decade, EVs have exhibited a trend of increasing e-motor speeds as a method of effectively increasing the power density of the motors, contributing to improved vehicle efficiency. The Nissan Leaf, a typical EV in 2010, had a maximum motor speed of 10,400 RPM, whereas the 2017 Tesla Model 3 and Toyota Prius Gen IV exhibit maximum motor speeds of 18,100 and 17,000 RPM respectively.⁸ This trend is expected to continue with EV motors predicted to reach 20,000 RPM and beyond in future models.^{8,9,10} These high speeds far exceed the capability of the lubricants used in internal combustion engine (ICE) vehicles and current EVs, and as a result, fluid technology has become a limiting factor in e-motor development.

Low viscosity lubricants will be required to facilitate the higher rotational speeds of motor bearings and simultaneously provide effective heat transfer away from the resulting higher temperature mechanical parts.¹¹ Without effective heat transfer, these parts, and the materials they interact with, could experience a steady decline in performance, and eventually lead to failures. Fluid design is even more crucial when the motor is located inside the transmission housing, as a single transmission fluid is required to satisfy the various tribological and thermal management requirements of the complex system. This configuration, known as a 'wet e-motor', is very common in hybrid electric vehicles (HEVs) as well as some full battery electric vehicle (BEV) designs. In environments such as this, EV fluids must also have suitable electrical conductivity as well as excellent compatibility with the wide variety of materials (from metal alloys to polymer seals).

Low-viscosity fluids generally achieve lower film thickness in lubrication applications, potentially leading to increased operating temperature and deterioration of parts due to friction.¹² Ionic liquids (ILs), however, are a unique class of fluids that can be designed to have low viscosities but also form protective tribofilms/layers on metal surfaces to combat the issue of wear. ILs exhibit many additional unique and desirable physical properties such as negligible volatility, a broad liquid range, high thermal stability, thermal conductivity, and heat capacity, as well as a wide electrochemical stability window.^{13,14,15,16,17,18,19} These properties make ILs ideal for use as EV fluids, having advantages over typically used mineral oils and synthetic fluids.

4. Electric Vehicles

Many varieties of EVs exist, with the two main categories being BEVs, describing vehicles powered exclusively by a battery, and HEVs which utilise battery energy storage combined with a secondary energy source – most commonly an ICE. BEVs have the advantage of not emitting GHGs when in use, and therefore, if charged by renewable electricity sources, have the potential to be carbon neutral. A review by Holmberg & Erdemir (2019) concluded that CO₂ emissions from ICE vehicles are 4.5 times higher (224 CO₂g/km) than a comparable BEV (50 CO₂g/km), powered by renewable energy, with the majority of the BEV emissions originating from the production stage.²⁰

EVs also operate with a significantly higher degree of efficiency when compared to ICE vehicles. An in-depth investigation into energy losses in passenger cars concluded that one-third of the fuel energy in ICE vehicles is lost in overcoming friction in the engine, transmission, tires, and brakes, whereas friction energy losses in EVs were found to be half this.²¹ This is in large part due to the elimination of idling losses in electric motors when the vehicles are temporarily stopped, and also due to the reduction of the number of gears and hence sources of friction. EVs also utilise regenerative braking technology to recover waste energy from braking and coasting to be stored for later use.²² This shows that phasing out ICE vehicles for EVs can be a viable solution to the task of reducing global GHG emissions.

4.1. Electric Motor Challenges

As motor speeds in EVs increase, more vehicles will require transmissions integrated into their drivetrain design. Placing the e-motor inside the transmission housing allows the sealed cavity to be flooded with transmission fluid which provides good thermal management and reduces foaming by preventing air from entering the system. It is noteworthy that once the fluid is added to this system, it must perform optimally for the EVs lifetime, without needing to be replaced. Automatic transmission fluids (ATFs) have existed for many years in ICE vehicles and are designed to meet a variety of requirements such as clutch friction durability, low temperature fluidity, anti-wear protection, and high resistance to oxidation.²³ However, having the e-motor in contact with the transmission in EVs poses new design challenges and extra considerations to be made. These include higher temperatures, more intense tribological demands, and electrical compatibility, unique to EVs.

If voltage differences are allowed to build between nearby internal components of the EV, current arcs and sparking may occur which can lead to malfunctions. E-motors can experience these voltage potentials between the shaft and the bearing housing, leading to increased temperatures and electrical wear (or 'pitting'), as well as safety issues.²⁴ In addition, fluids in contact with the electrical windings in the stator, must possess low electrical conductivity to prevent a short-circuit.²⁵ The lubricants therefore should not be insulating, since this could promote static build-up, leading to subsequent discharges.⁷ For these reasons, it is important that charges are allowed to dissipate in a controlled manner. As charge carrying species, ILs would likely be effective in this role, particularly as it is possible to tailor electrical conductivity to an appropriate level through structural design synthesis.

4.1.1 Thermal Management of E-motors

An effective, integrated thermal management system is an essential aspect of e-motor innovation, as aforementioned. Heat dissipation is crucial in meeting performance targets and ensuring that the e-motor components such as motor windings have a long lifespan.²⁶ The main heat sources of e-motors are located in the bearings where mechanical friction occurs, the copper coil windings where high current is passed, the copper core, and in the interior RE-PM. It is vitally important that as power density, rotational speeds, and torque of e-motors increase (including at low cruising speeds), the temperature of the motor parts are reduced to avoid demagnetisation.²⁷ This occurs at 150 °C in the Nd magnets and 180 °C in the C class copper coils, with the most critical temperature locations being in the rotor where the RE-PM is located, and in the stator where the coil is wound.²⁷ The major contributor to motor power loss (approximately 50%) is attributed to copper loss in the core, which is proportional to the temperature.¹¹ In effect, keeping the temperature of motor windings below the 150 °C limit significantly improves motor efficiency.²⁸

There are a wide range of techniques that can be employed to cool a high temperature system including: air cooling, indirect liquid jacket cooling, phase-change cooling, and direct liquid cooling.²⁸ Air cooling is effective in lower power density motors, however due to the poor thermodynamic properties of air it is not efficient in the high density motors that this research is targeted.²⁸

Direct liquid cooling of the heat source is the most effective method, enabling higher current loading capacity and as a result higher power density of the e-motors.^{29,30} For example, a prototype direct liquid cooling design by Lindh et al. (2019) was successful in keeping PM motor winding operational temperatures consistently below 80 °C by flowing coolant through hollow passages in the stator windings.³¹ Despite this being an effective heat removal method, in practice such methods may not be viable due to the complex manufacturing of motors with integrated direct liquid cooling channels such as this. It is therefore advantageous to design an EV fluid that can be in direct contact with motor components without the need for reengineering of the motor itself.

An effective heat transfer fluid should have the following attributes:^{23,32}

- **High thermal conductivity** – to ensure efficient transfer of heat into the fluid from the heat source.
- **High heat capacity** – so that the fluid can store significant thermal energy per unit mass.
- **High density** – to ensure the fluid has a high carrier mass per unit volume to enable greater per volume absorption of heat.
- **Low viscosity** – so that the fluid has a low resistance to flow and can dissipate the heat away from the source quickly.
- **High thermal stability** – to prevent degradation of the fluid and subsequent loss of heat transfer ability.

4.1.2. Tribological Demands of Wet E-motors

Volatilisation of lubricant can occur at high temperatures, leading to high contact wear.³³ Since EV motors produce higher torque, compared to ICE, and maximum power can be provided, even at slow speeds, the tribological demands of the vehicles are much more intense.³⁴ The specific areas requiring the most targeted lubrication are the transmission gears and rolling bearings and brushes/slip rings in the e-motor.⁹ Small friction losses of individual bearings can contribute to significant energy losses and increased fuel consumption of the vehicle.³⁵

Table 1 - API base oil categorisation.^{36,37}

Base Oil Group	Production Method	Sulphur Content (%)	Saturate Content (%)	Viscosity Index (VI)
I	Solvent refined crude oil	>0.03%	<90%	80≤VI<120
II	Hydrocracked crude oil	≤0.03%	>90%	80≤VI<120
III	Hydrocracked crude oil	≤0.03%	>90%	120≤VI
IV	Synthetic	-	100%	120≤VI

Base oils are typically used in vehicles to combat friction and improve efficiency. The American Petroleum Institute (API) categorisation of base oils can be seen in Table 1. Group I base oils contain a significant amount of sulphur, saturates and aromatics which is detrimental to lubricant performance.³⁸ Although improvements are shown in group II and III oils, which are used in ICE vehicles, they are unsuitable for use as high performance lubricants due to their low VI values and volatilisation at high temperatures.

Group IV base oils are poly-alpha-olefins (PAOs). These are fully saturation synthetic oils, with a high VI range and low pour point (PAO4 = -30 °C), making them ideal for use as lubricants over wide temperature ranges.³⁸ PAOs are already utilised as high performance lubricants and can also be applied as heat transfer fluids.³⁹ An additional advantage of this base oil group is that they are considered non-toxic and anti-irritant, as well as demonstrating higher levels of biodegradation than equivalent viscosity mineral oil grades.³⁹ This makes them a lot more environmentally considerate than alternative base oil groups. For these reasons, PAO oils are being widely considered as an alternative to the motor oils used at present, particularly due to their low viscosity nature.³⁴

5. Ionic Liquids

ILs have drawn huge interest in the scientific community since their discovery, finding applications in catalysis, electrochemistry and specialist solvents systems.^{40,41,42,43} ILs were first discussed as potential advanced lubricants in 2001.⁴⁴ Numerous tribological and thermophysical studies have since been conducted, confirming that IL based lubricants can provide excellent anti-wear and friction reduction properties in conjunction with high stability over wide temperature ranges. As a result of their excellent thermophysical properties, ILs have also been considered for use as heat transfer fluids since the beginning of the century as well as thermal storage fluids in renewable solar energy capture.^{45,46,47} There is potential to combine these applications in new generation EVs by using ILs as lubricating fluids that simultaneously regulate the temperature of mechanical and electrical components through heat transfer and dissipation.

An attractive quality of ILs is the ability to tailor the bulk physical properties of the chemicals by making modifications to the ionic components. ILs are most commonly composed of an organic cation and a non-coordinating inorganic anion, both of which can be customised to achieve a wide variety of properties. For example, the $[C_4mIm]^+$ cation gives an IL with a melting point of 70 °C when paired with a chloride anion, however by substituting this for a $[NTf_2]^-$ anion, the melting point falls to -4.15 °C.^{48,49} Interestingly, minor structural alterations to a cation species, such as lengthening a branched hydrocarbon chain, allows for much finer tuning of the physical properties. Therefore, anion selection and cation modification can be utilised to obtain very stable, low viscosity fluids with a broad liquid range, aligning with the requirements of new classes of EV fluids.

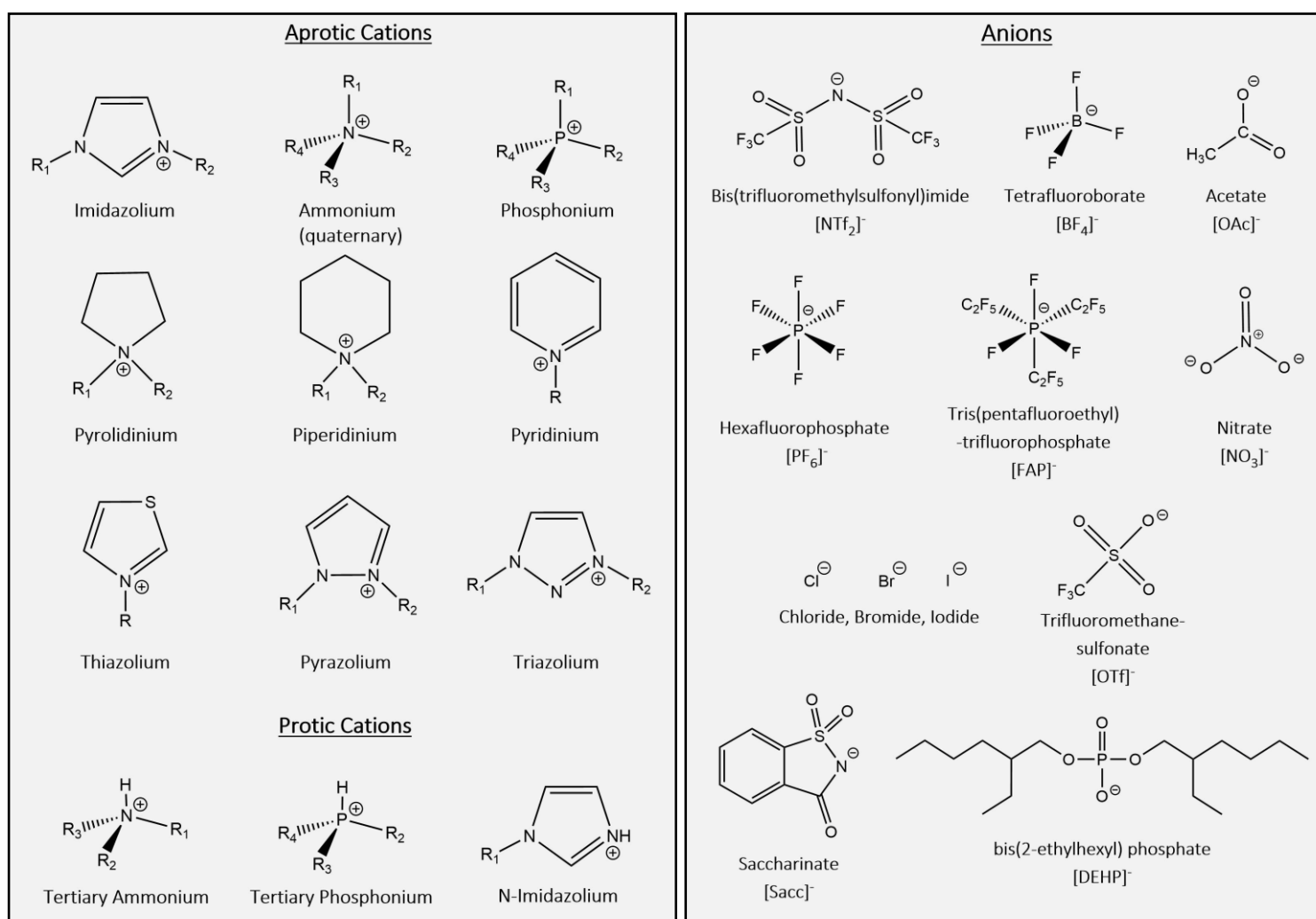


Figure 1 – Common Ionic Liquid Structures

As seen in Figure 1., there are a wide range of cationic and anionic species that can be combined to create an IL. It has been estimated that there are approximately 10^{18} possible unique IL systems can be synthesised, and therefore, there is an endless supply of potential research avenues to explore.⁵⁰

5.1 Cationic Structures

The cation species in ILs are the components that offer the most opportunity for modifications, as a result of being organic molecules, often with customisable alkyl substituents. Additional functionality can be easily added to these structures with functional groups such as benzene, ether or alcohol groups. However, it is the inherent framework of the cation that provides the dominant physical properties. Therefore, careful selection is needed, beginning with the subcategory of cation.

5.1.1 Aprotic Monocations

The most widely studied class of ILs are aprotic monocationic ILs such as imidazolium, pyrrolidinium, pyridinium, piperidine, triazolium, phosphonium and ammonium-based species. Common synthesis methods involve a nucleophilic substitution reaction to obtain the desired cation, followed by an anion exchange reaction (such as a metathesis reaction) to substitute the anion species to achieve desired physical properties. This relatively straightforward synthesis enables a huge variety of cations with differing substituent lengths to be produced and studied, enabling the expansive collection of research on the topic. In terms of tribological and thermal fluid research, this is the dominant class of cation found in the existing publications, with imidazolium cations particularly being researched extensively, due to the often-high thermal stability of these ILs.

Aprotic ILs such as phosphonium phosphate have been shown to successfully coexist in PAO6 base oil with other additives including antiwear oxide nanoparticles (ZnO) and the commercial dispersant PIBSA, resulting in 50% wear reduction.⁵¹ This has huge incentives for commercialisation as they can be used in small quantities and work in synergy with existing additives in base oil stocks.

5.1.2 Protic Monocations

Protic ILs (PILs) are a subcategory of ILs which are formed by the transfer of a H^+ from a Bronsted acid to Bronsted base in a neutralisation reaction.^{13,52} The First IL, discovered by Walden in 1914, was the PIL $[EtNH_3][NO_3]$, with a melting point of less than $12\text{ }^\circ\text{C}$.⁵³ As a result of this simple synthesis, often without the need for solvent media, PILs are generally low in cost, particularly in comparison to other ILs. In addition to this, 100% atom economy is achieved, adhering to the classical principles of green chemistry.⁵⁴ The most common PILs include tertiary ammonium species, however primary and secondary ammonium, as well as phosphonium species have been studied for specialised applications.⁵⁵ PILs generally exhibit lower glass transition temperatures than their most equivalent aprotic ILs (such as quaternary ammonium salts when compared with equivalent tertiary ammonium species), making them suitable for use in low temperature environments.⁵⁶ This is a desirable quality as EVs must be operational in a wide range of climates, including countries that experience consistently low temperatures.

Notable strengths of PILs appear to be in surface wear reduction and their solubility in non-polar oils, making them effective performance enhancing additives. Much like aprotic ILs, functionalised substituents can be integrated into the chemical structure to facilitate specified functions or to

achieve desirable physical properties. The hydroxy substituents on Di-[bis(2-hydroxyethyl) ammonium] adipate have been shown to bind to metal surfaces through H-bonding leading to significant reductions in abrasive wear (a 34% reduction from a 1 wt% additive of the PIL in PAO6).⁵⁷

However, increased H-bonding results in greater viscosity and melting point, and a careful balance must be negotiated between these properties.

Studies have shown many PILs to be non-toxic and bio-compatible, making them environmentally favourable to other ILs, particularly those containing fluorine.^{55,58} More recently, tertiary ammonium PILs with long hydrocarbon chains, paired with bulky [NTf₂]⁻, carboxylate and phosphate anions have shown promising results as base oil additives and use as lubricants, leading to significant reductions in friction.^{59,60,61} In a study comparing tributyl ammonium and phosphonium ILs, phosphonium analogues displayed superior thermal stability and a wider liquid range.⁵²

5.2.3 Dicationic ILs

Dicationic ILs (DILs) are a newer class of ILs which have shown superior thermal stability compared to conventional ILs, making them ideal candidates for use in EVs.⁶² They were first considered as potential high temperature lubricants in 2006 after investigations showed that functionalised polyethylene glycol imidazolium DILs exhibited excellent tribological performance at temperatures as high as 300 °C.⁶³ Their general structure consists of a cation with two positive charge groups, often paired with two independent single-charged anions (dicarboxylate anions have been paired with dications, yet show lower stability).⁶⁴

DILs can be either geminal (where both cationic moieties are the same), or asymmetric where different positive charge groups are used. These liquids open the door for even finer tuning of properties than is possible for monocationic ILs as the alkyl groups on the cation ends can be varied as well as the length and functionality of the linkage chain between them. Asymmetric DILs offer lower melting points due to greater disorder and difficulty in forming a structured lattice, making them appealing for use in low temperature environments.⁶⁵ However, this also leads to slightly lower thermal stability and higher viscosities when compared to geminal DILs, making asymmetric DILs less appropriate for high temperature functions.^{66,67}

Another disadvantage of asymmetric DILs is the complexity of their synthesis and difficulty in achieving high yields. Currently there is a lack of well-established, effective synthesis methods for many of these dications as difficulties often arise in isolating the mono-substituted alkyl-halide intermediate before further substitutions take place. The most practiced method involves reaction with the dihaloalkane in large excess (1:8 ratio with imidazole/pyrrolidine reactant) at low temperature, using a substantial volume of solvent. This results in extremely low yields, a significant volume of waste solvent and the need for intensive purification of the intermediary product, making the process discordant with the practices of Green Chemistry and economically unfavourable. Contrary to this, effective synthesis methodology has been established for pyridine DILs. This is due to the pyridine having low nucleophilicity and as a result, only a single bromide is substituted at low temperatures, thus achieving higher yields (up to 99%).⁶⁸ Despite this, asymmetric pyridinium DILs haven't been found to exhibit as desirable thermophysical properties as geminal dicationic imidazolium and pyrrolidinium DILs.

5.2.4 Poly-ILs

IL polymers (poly-ILs) have been a growing area of interest, with some species showing impressive characteristics of low temperature glass transitions and high thermal stability – such as poly(1,2,3-triazolium) poly-ILs with T_g in the range -42 to -25 °C and $T_d(10\%)$ of 308 to 369 °C.⁶⁹ Imidazolium Poly-ILs, however, have been shown to exhibit much higher melting points than imidazolium DILs, with poly-hexylimidazolium $[\text{NTf}_2]^-$ melting at 50 °C, compared with $[\text{C}_5(\text{C}_4\text{Im})_2][\text{NTf}_2]^-$ which displayed a glass transition at -61 °C with no obvious crystallisation behaviour.⁷⁰ The researchers found that this problem could be solved by using the DIL as a low percentage additive (4 wt%) in the poly-IL, leading to a single glass transition at -45 °C being observed. Poly-ILs also exhibit dramatically improved wear and friction reduction properties due to their robust strength and strong adhesion to solid surfaces.⁷¹ However, the impressive tribological behaviour is the result of high viscosity films that form on surfaces which may not be appropriate for lubricating fast moving mechanics in EVs. Similarly to conventional polymers, poly-ILs have been found to exhibit shear-thinning viscosity behaviour as opposed to the Newtonian fluid behaviour commonly displayed by ILs.¹⁴ For example, the aforementioned poly-hexylimidazolium $[\text{NTf}_2]^-$ displayed an extremely high viscosity of 19,054 Pa·s at 25 °C which reduced to just 82 Pa·s with increased shear rate.⁷⁰ However, even under high shear these viscosities are far higher than those of monocationic and dicationic ILs, making Pol-ILs likely more suited to the lubrication of slower-speed contact systems where a grease-like material is more appropriate.

5.2. Anion Selection

Anion selection can have the most significant influence on the overall properties of the ILs such as thermal stability, viscosity, and water solubility, as well as the ILs tribologically beneficial surface interactions.⁷² Common anion species can be seen in Figure 1.

$[\text{BF}_4]$ and $[\text{PF}_6]$ imidazolium salts are widely studied due to being relatively cheap. However, they are hydrophilic and can cause unfavourable reactions with water, undergoing hydrolysis to form HF gas, which is highly corrosive and toxic.^{73,74} Therefore, these anions should not be considered for use in future vehicles due to safety and environmental concerns.

$[\text{NTf}_2]^-$ however, is significantly more hydrophobic than other fluorine containing anions and boasts many favourable properties when combined with an appropriate cation, including high thermal stability, broad liquid range, effective anti-wear properties and low viscosity.^{75,76}

5.3. Anti-Wear and Friction Reduction Properties of ILs

A unique property of ILs is their ability to interact with metal surfaces to form protective tribolayers. This occurs readily due to existing in ionic form, contrasting popular anti-wear additives such as zinc dithiophosphate (ZDDP) which needs high contact pressure or elevated temperature to be broken down before the surface interaction can occur.⁷⁷ It is often the anion species that carries out this interaction, especially in the case of fluorine containing anions, due to high reactivity.

When used as neat lubricants, ILs are shown to exhibit the most effective anti-wear and friction reduction effects. However, significant reductions can be made when ILs are used as additive species in a base oil fluid. González *et al.* (2010) observed that notable friction reduction occurred in ball-on-plate experiments of TiN, CrN and diamond-like carbon coated surfaces when only 1 wt% (1-butyl-1-

methylpyrrolidinium tris(pentafluoroethyl)trifluorophosphate ($[C_4(C_1\text{Pyrr})][FAP]$) additive in PAO6 was used.⁷⁸ Although less of a friction reduction was seen than the neat IL, it performed far more effectively than the neat PAO6. Similarly, Pejakovic *et al.* (2012) employed pyrrolidinium sulfate and ammonium sulfate ILs as additive species in steel-steel contact lubrication and found that the optimum concentration for wear reduction was 0.625%. These low concentration IL investigations show incredibly promising results, providing an elegant solution to the high costs of ILs, if similar benefits can be achieved using significantly lower amounts. Using ILs as additives may also reduce dependency on anti-wear additives, surfactants, dispersants, detergents, antioxidants and friction modifiers in lubricant base oils as one single additive may be able to carry out many of these functions.⁷⁹

In fact, in higher temperature environments popular anti-wear additives, such as ZDDP, are found to become less effective. Research by Qu *et al.* (2014) found that ZDDP failed to prevent scuffing at high temperature (100 °C), however, the $[P_{66614}][DEHP]$ IL maintained a stable tribofilm, resulting in a much lower wear rate.⁸⁰ It is therefore clear that advancements in anti-wear additives are required to operate in the higher temperatures of EV motors. High stability ILs appear to be an ideal fit for this function. It has been observed that when anion species contain a longer alkyl chain length, better anti-wear and friction reduction performance is achieved since the longer chains provide greater separation of metal contacts.⁸¹ This is a strong hypothesis for why ILs such as $[P_{66614}][DEHP]$ exhibit such effective anti-wear performance.

5.4 Barriers to Commercialisation

The main barrier of the commercialisation of ILs is the high economic cost of production. It has been suggested that the cost of ILs is still too high for big industry applications, such as metal machining and refinement and that using ILs as additive species in mineral lubrication oils is a more economical solution.⁸² The most expensive component of ILs that are suitable for this application is usually the anion, with the $[NTf_2]^-$ anion being the highest cost of conventional anion species.⁸³ However, multiple industrial applications have been employed in real-world settings over the past decade ranging from use as a solvent in the BASF(biphasic acid-scavenging utilising ionic liquids) process, and Mettop GmbH's collaboration with Proionic to produce ILTEC cooling technology, directly substituting water with an equal viscosity IL to achieve more efficiency in heat transfer applications.⁸⁴

In a 2009 economic study, it was concluded that ILs are unlikely to replace current heat transfer fluids in the near future as the cost of redesigning the technology and providing enough fluid to fill the system would be too costly at the current rate of production.⁸⁵ However, ILs are now more readily available being currently manufactured by large chemical companies such as IoLiTec, Merck, Cytac and BASF.⁸² As production continues to grow, prices are expected to fall.

In addition, new industrial synthesis methods are being developed such as CBILS[®] (Carbonate-Based Ionic Liquid Synthesis) which can reduce costs and the environmental impacts of production. CBILS[®] is a halide-free synthesis method for producing pure imidazolium, pyrrolidinium, and phosphonium-based ILs, such as 1,3-dialkylimidazolium based ILs.⁸⁶ To obtain this imidazolium IL, firstly the intermediate 1-alkylimidazole is synthesised by alkylating a 1H-imidazole at temperatures of 80 – 130 °C using a non-hazardous dialkylester of carbonic acid (R_2CO_3). The 1-alkylimidazole is then reacted under inert gas with another carbonic acid dialkylester (R'_2CO_3) in a corresponding alcohol ($R'OH$) solvent to form 1,3-dialkylimidazolium alkylcarbonate.⁸⁶ The formed byproducts CO_2 and the alcohol can be recycled back to the carbonic acid dialkylester, eliminating waste material. A simple

anion metathesis then yields the final IL product. The CBILS[®] method can be implemented as a continuous flow industrial manufacturing process, significantly reducing operating costs and boosting efficiency, making industrial IL production more achievable.⁸⁷

6. Experimental

A series of ILs were synthesised following an extensive investigation into globally published research up until the current date, predominantly using article search engines such as Web of Science and Google Scholar. This investigation began with a focus on ILs that have been shown to perform well tribologically at high temperatures, such as Imidazolium and Pyrrolidinium [NTf₂] ILs, and spanned the research summarised in **section 4**. The high temperature performance was crucial because of the aforementioned high rotational speeds of the moving parts in electric motors and the resulting high temperature environment of the target functions for the liquids in this study. In addition to this, a range of physical property data relating to previously studied ILs was reviewed, including melting points, thermal conductivity, and viscosity, as to determine which structural design aspects of the molecules provided the desired physical properties for the context of use in EVs. This informed which experimental routes to pursue by expanding on recent research. This included synthesising and studying new DILs with extended alkyl chains and providing more thermophysical data for species that had shown promising tribological performance in previous studies, such as [N_{888H}][DEHP].

The research aided in determining the ILs that showed the most potential as effective high-performance EV fluids and identified where there was missing physical property data that it would be beneficial to collect. This would allow for a more holistic analysis of the suitability of these fluids in this application.

The physical properties measured in this study include phase transitions (melting points and glass transitions), thermal stability (degradation onset and 1% degradation temperatures), heat capacity over a wide temperature range, viscosity (dynamic and kinematic), and density.

The suitability of the IL species as additives in high performance PAO base fluids was also investigated, as well as the influence of different IL concentrations on the thermophysical properties of the resulting fluids. This was important to include in the investigation as real-world application of these fluids is arguably more likely to be firstly adopted as additive ingredients as opposed using them neat. This is because it is more economical feasible – since ILs are much more expensive than base oil stocks, and additionally because EV motors are well established, meaning that greater mechanical redesign would possibly be required to completely replace currently used motor oils with novel fluids.

6.1 Synthesis and Characterisation

All ILs were prepared with dry distilled reagents under inert atmospheres, using standard Schlenk line techniques. ¹H, ¹³C and ¹⁹F NMR spectra were measured using a Bruker Advance III 400HD (400 MHz) Nuclear Magnetic Resonance Spectrometer and samples were prepared in *d*₆-DMSO unless stated otherwise. Spectra were referenced to the residual solvent peaks (e.g., *d*₆-DMSO ¹H NMR = 2.50 ppm and ¹³C NMR = 39.52 ppm).⁸⁸

Further characterisation was conducted with a Bruker microTOF II High Resolution Mass Spectrometer with an electrospray ionisation source in the range of 50 – 20,000 *m/z*. Samples were prepared at a concentration of ~0.1 mg cm⁻³ using HPLC-grade methanol solvent. The instrument was recalibrated to reduce the errors when measuring ILs at low *m/z*. Since the synthesised dications have a 2+ charge, the *m/z* of these species is half the molecular weight, putting the signals at the low end of the measured range. Chem Draw's *m/z* estimation tool was used to predict the ionization peaks of the mass spectrum and was used to aid characterisation. This method was particularly useful in identifying the presence monocationic impurities in the geminal dicationic liquids.

1-Butyl-3-methylimidazolium Bromide, [C₄(C₁Im)]Br

Synthesised via a method adapted from *Liu et al. (2011)* and *Weber et al. (2012)*.^{89,90}

Prior to the reaction, 1-bromobutane was distilled at 93.5 °C under atm pressure to give a colourless liquid (80% yield). 1-Methylimidazole was distilled under reduced pressure from CaH₂ by Matthew Palmer. Under inert Ar gas, 1-bromobutane (23.5 mL, 0.22 mol) was added dropwise to N-methylimidazole (16 mL, 0.20 mol) in anhydrous acetonitrile (100 mL). The mixture was stirred at room temperature for 30 min, followed by heating at 50 °C for 12 h. After completion, ethyl acetate (150 mL) was added slowly until the mixture began turning cloudy. The mixture was cooled in a freezer overnight, yielding white crystals which were isolated via filtration under reduced pressure and dried for 12 h under vacuum (2.6 x 10⁻² mbar) at 70 °C. [C₄(C₁Im)]Br (39.94 g, 182.3 mmol, 91%, m.p. 73.7 °C). ¹H NMR (400 MHz, DMSO) δ 9.31 (s, J = 1.8 Hz, 1H), 7.84 (apt. t, J = 1.8 Hz, 1H), 7.76 (apt. t, J = 1.8 Hz, 1H), 4.19 (apt. t, J = 7.2 Hz, 2H), 3.87 (s, 3H), 2.08 (s, 0H), 1.76 (p, J = 7.4 Hz, 1H), 1.24 (h, J = 7.4 Hz, 2H), 0.88 (t, J = 7.4 Hz, 3H). ¹³C NMR (101 MHz, DMSO) δ 136.44, 123.37, 122.15, 48.27, 40.14, 39.94, 39.73, 39.52, 39.31, 39.10, 38.89, 35.74, 31.31, 18.62, 13.17.). **MS (ESI +)** (m/z (%)): 139.1235 (100) ([C₄C₁Im]⁺), 140.1265 (9.9). **1-Butyl-3-methylimidazolium Bis(trifluoromethylsulfonyl)imide, [C₄(C₁Im)][NTf₂]**

Metathesis anion exchange reactions were based on the method published by *Anderson et al. (2005)*.⁶²

A solution of LiNTf₂ (48.80 g, 0.17 mol) in water (50 mL) was added to a solution of [C₄(C₁Im)]Br (20.25 g, 0.15 mol) in dichloromethane (100 mL) and stirred vigorously at room temperature for 24 h. The lower IL layer of the biphasic mixture was extracted and washed repeatedly with water (10 x 50 mL). The solvent was removed from the colourless ionic liquid product under vacuo. (2 h at 30 mbar pressure), then dried under vacuum at 70 °C and 1.4 x 10⁻² – 3.0 x 10⁻³ mbar overnight, yielding [C₄(C₁Im)][NTf₂] (62.5 g, 0.15 mol, 99%). ¹H NMR (400 MHz, DMSO) δ 9.10 (d, J = 1.8 Hz, 1H), 7.77 (apt. t, J = 1.8 Hz, 1H), 7.70 (apt. t, J = 1.8 Hz, 1H), 4.16 (t, J = 7.2 Hz, 2H), 3.85 (s, 3H), 1.83 – 1.71 (m, 2H), 1.34 – 1.20 (m, 2H), 0.91 (t, J = 7.3 Hz, 3H). ¹³C NMR (101 MHz, DMSO) δ 136.96, 124.09, 122.74, 121.55, 48.97, (DMSO: 40.62, 40.41, 40.20, 39.99, 39.79, 39.58, 39.37), 36.21, 31.81, 19.23, 13.71. ¹⁹F NMR (376 MHz, DMSO) δ -78.78. **MS (ESI +)** (m/z (%)): 139.1233 (100) ([C₄C₁Im]⁺), 140.1262 (9.9).

1,10-Bis(3-methylimidazolium-1-yl)decane Dibromide, [C₁₀(C₁Im)₂]Br₂

Synthesised based on methods described in the literature.⁹¹

1-10-dibromodecane was recrystallised before use in min volume of chloroform to give large white crystals which were dried under vacuum (~20 mbar) for 2 h. 1-10-Dibromodecane (18.66 g, 62 mmol) was dissolved in dry acetonitrile (100 mL) and stirred under inert Ar gas for 2 min. 1-methylimidazole (10 mL, 125 mmol) was added slowly and the mixture was refluxed at 70 °C for 72 h. Upon completion, diethyl ether was added dropwise until the solution remained cloudy, and the mixture was cooled in a freezer overnight, forming small white crystals. The crystals were isolated and washed with diethyl ether (5 x 10 mL) and dried under vacuum (50 °C, 7x10⁻² mbar, 24 h), yielding [C₁₀(C₁Im)₂]Br₂ (22.89 g, 59.9 mmol, 96.62 %, m.p. 145.6 °C). ¹H NMR (400 MHz, DMSO) δ 9.16 (s, 2H), 7.78 (t, J = 1.8 Hz, 2H), 7.71 (t, J = 1.8 Hz, 2H), 4.15 (t, J = 7.2 Hz, 4H), 3.85 (s, 6H), 1.77 (p, J = 7.3 Hz, 4H), 1.30 – 1.20 (m, 12H). ¹³C NMR (101 MHz, DMSO) δ 136.48, 123.60, 122.26, 48.74, 35.76, 29.39, 28.77, 28.38, 25.51. **MS (ESI +)** (m/z (%)): 152.1309 (100), 152.6324 (22).

1,10-Bis(3-methylimidazolium-1-yl)decane Bis(trifluoromethylsulfonyl)imide, [C₁₀(C₁Im)₂][NTf₂]₂

Synthesis was adapted from the method outlined by *Haines et al. (2020)*.⁹²

[C₁₀(C₁Im)₂Br₂] (10.0 g, 21.5 mmol) was dissolved in deionised water (20 mL). To this, a solution of LiNTf₂ (15.0 g, 51.7 mmol) in deionised water (20 mL) was added and the resulting mixture was stirred vigorously (20 °C, 24 h). Ethyl acetate (10 mL) was added to reduce viscosity of the organic layer, and the mixture was stirred vigorously for 10 min before leaving to stand, allowing the layers to separate. The organic layer was extracted and washed with deionised water (10 x 50 mL) until a silver nitrate test no longer indicated presence of Br⁻ ions. The solvent was removed, yielding a colourless, oil-like liquid [C₁₀(C₁Im)₂][NTf₂]₂ (16.04 g, 18.5 mmol, 86.2%) which was dried under 7.2x10⁻³–4.0x10⁻² mbar pressure (50 °C, 24 h). ¹H NMR (400 MHz, DMSO) δ 9.08 (s, 2H), 7.74 (t, *J* = 1.8 Hz, 2H), 7.68 (t, *J* = 1.8 Hz, 2H), 4.14 (t, *J* = 7.2 Hz, 4H), 3.84 (s, 6H), 1.77 (p, *J* = 7.5 Hz, 4H), 1.25 (s, 12H). ¹³C NMR (101 MHz, DMSO) δ 136.47, 124.29, 123.61, 122.24, 121.09, 117.89, 114.70, 48.79, 35.72, 30.63, 29.40, 28.77, 28.38, 25.52. **MS (ESI +)** (*m/z* (%)): 152.1317 (100), 152.6330 (21.3), 153.1344 (2.3).

1,10-Bis(methylpyrrolidinium) Dibromide, [C₁₀(C₁Pyrr)₂]Br₂

1-methylpyrrolidine was distilled at 80 °C under atmospheric pressure (vapour temperature: 77-79 °C, 80% yield), giving a colourless distillate.

1-10-dibromodecane (16.95 g, 57 mmol) was dissolved in dry acetonitrile (100 mL) with moderate stirring. 1-methylpyrrolidine (12.6 mL, 118 mmol) was added slowly and the solution was refluxed (50 °C, 42 h). A white precipitate formed after 15 min, later becoming a solid, thick white crust on the surface of the reaction whilst the reaction mixture had a yellow colouration. Upon completion, the precipitate was isolated from the reaction mixture via filtration and was recrystallised in minimum volume of hot acetonitrile, using cold diethyl ether as the antisolvent. The bright white waxy solid was washed with cold ether and dried under reduced pressure (< 10⁻² mbar, 24 h) to yield the pure dibromide salt (21.47 g, 45.6 mmol, 80%). ¹H NMR (400 MHz, DMSO) δ 3.54 – 3.37 (m, 8H), 3.35 – 3.26 (m, 4H), 2.98 (s, 6H), 2.08 (p, *J* = 3.5 Hz, 8H), 1.69 (dp, *J* = 15.0, 5.4 Hz, 4H), 1.39 – 1.17 (m, 12H). ¹³C NMR (101 MHz, DMSO) δ 63.36, 62.99, 47.45, 28.77, 28.52, 25.94, 22.95, 21.06. **MS (ESI +)** (*m/z* (%)): 155.1665 (100), 155.6681 (23.9), 156.1695 (2.6).

1,10-Bis(methylpyrrolidinium)decane Bis(trifluoromethylsulfonyl)imide, [C₁₀(C₁Pyrr)₂][NTf₂]₂

[C₁₀(C₁Pyrr)₂]Br₂ (21.22 g, 55.1 mmol) was dissolved in deionised water (200 mL). To this, a solution of LiNTf₂ (36.32g, 126.5 mmol) in deionised water (100 mL) was added and the resulting mixture was stirred vigorously (20 °C, 24 h). The aqueous layer was removed, and ethyl acetate (30 mL) was added to the pale-yellow IL to decrease viscosity. The IL layer was washed repeatedly with deionised water (5 x 50 mL) until a silver nitrate test on the aqueous layer indicated no presence of Br⁻. The solvent was removed under vacuum (8 mbar, 2 hr) with further drying on a Schlenk line (< 10⁻¹ mbar, 24 h) leaving the product as a pale-yellow viscous liquid, [C₁₀(C₁Pyrr)₂][NTf₂]₂ (37.3 g, 39.4 mmol, 71.6 %). ¹H NMR (400 MHz, DMSO) δ 3.53 – 3.33 (m, 5H), 3.30 – 3.22 (m, 3H), 2.97 (s, 6H), 2.13 – 2.00 (m, *J* = 5.8, 5.3 Hz, 8H), 1.68 (tt, *J* = 10.8, 6.7 Hz, 4H), 1.29 (t, *J* = 5.2 Hz, 13H). ¹³C NMR (101 MHz, DMSO) δ 119.48 (q, *J* = 322.0 Hz), 63.39, 63.08, 47.46, 28.78, 28.53, 25.93, 22.94, 21.06. **MS (ESI +)** (*m/z* (%)): 155.1673 (100), 155.6687 (21.3), 156.1702 (2.7).

N-octylimidazole

Imidazole (20.0 g, 293.8 mmol) was dissolved in dry THF (200 mL) under an inert Ar atmosphere and NaH (7.05 g, 293.8 mmol) was added dropwise via an addition funnel, taking care to avoid any sudden raises in temperature. Once the NaH had completed reacting, and the production of H₂(g) halted, the mixture was stirred for a further 1 h at room temperature ensuring complete production of the sodium imidazolite salt. 1-bromooctane (56.8 g, mmol, 50.6 mL) was dissolved in dry THF (50 mL) and added slowly to the solution. After 2 h the mixture was heated to reflux (75 °C) and stirred for 24 hr. The mixture was cooled and filtered, extracting the organic solution from the insoluble solid sodium bromide salt. The solvent was removed under reduced pressure, yielding a dark orange liquid which was purified via distillation (6x10⁻³ mbar, 92 °C), giving pure N-octylimidazole (41.14 g, 228.16 mmol, 78.7 %). ¹H NMR (400 MHz, DMSO) δ 7.59 (s, 1H), 7.13 (t, J = 1.4 Hz, 1H), 6.87 (s, 1H), 3.92 (t, J = 7.1 Hz, 2H), 1.68 (p, J = 7.2 Hz, 2H), 1.28 – 1.15 (m, 10H), 0.85 (t, J = 6.8 Hz, 3H). ¹³C NMR (101 MHz, DMSO) 137.63, 128.27, 119.14, 45.88, 31.17, 31.00, 30.58, 28.58, 28.54, 28.52, 28.51, 28.49, 28.48, 28.43, 26.07, 25.92, 22.21, 22.14, 22.04, 22.00, 21.94, 21.87, 13.90.

1,10-bis(3-octylimidazolium-1-yl)decane Dibromide, [C₁₀(C₈Im)₂]Br₂

1-10-dibromodecane (16.50 g, 55.0 mmol) was dissolved in dry acetonitrile (100 mL) and stirred under inert Ar gas for 2 min. N-octylimidazole (20 mL, 122 mmol) was added slowly and the mixture was refluxed (85 °C, 72 h). Upon completion, cold diethyl ether (~20 mL) was added to the solution until it became cloudy, and crystallisation occurred via cooling in a freezer overnight. The product was isolated and washed with cold diethyl ether, under a stream of N₂ gas, yielding a sticky white solid. The remaining solvent was removed *in vacuo* and the product was recrystallised, repeating the method above. The final product was dried under vacuum (50 °C, 10⁻² mbar) giving a bright white free-flowing powder (4.4 g, 6.66 mmol, 12.1 %). Washings were recovered and recrystallised, however, remained contaminated with a monocation impurity. ¹H NMR (400 MHz, DMSO) δ 9.33 (s, 2H), 7.84 (d, J = 1.6 Hz, 4H), 4.17 (t, J = 7.1 Hz, 8H), 1.83 – 1.74 (m, 8H), 1.32 – 1.14 (m, J = 6.8 Hz, 34H), 0.84 (t, J = 6.7 Hz, 6H). ¹³C NMR (101 MHz, DMSO) δ 135.93, 122.46, 48.83, 31.12, 29.30, 29.24, 28.81, 28.48, 28.37, 28.27, 25.52, 25.45, 22.04, 13.93. **MS (ESI +)** (m/z (%)): 250.2408 (100), 250.7423 (37.1), 251.2437 (7.1).

1,10-Bis(3-octylimidazolium-1-yl)decane Bis(trifluoromethylsulfonyl)imide, [C₁₀(C₈Im)₂][NTf₂]₂

LiNTf₂ (4.06 g, 14.2 mmol) was dissolved in deionised water (20 mL) and added directly to [C₁₀(C₈Im)₂]Br₂ (4.25 g, 6.43 mmol) in deionised water (50 mL). The reaction mixture was then vigorously stirred at room temperature for 24 h, leading to the formation of a colourless viscous liquid that was insoluble in the aqueous solution. The aqueous layer was removed, and the IL was extracted with ethyl acetate (~10 mL) before being washed several times with deionised water (5 x 20 mL).

Unfortunately, the product became contaminated by another IL during this stage and separation was unsuccessful.

1,3-Bis-(N-octylimidazolium-1-yl)xylene Dichloride, [m-xyl-(C₈Im)₂]Cl₂

Synthesis method adapted from that described in the literature.⁹³

N-octylimidazole (16.38 g, 90.85 mmol) was added dropwise to a solution of meta-xylene dichloride (7.23 g, 41.30 mmol) in dry acetonitrile (100 mL). The reaction mixture was stirred vigorously and heated to 85 °C for 24 h, after which the temperature was increased to 95 °C for a further 24 h. Upon completion, the solvent was removed *in vacuo* (~150 mbar) giving an orange viscous liquid which was washed with diethyl ether (50 mL). The mixture was allowed to settle, and the diethyl ether was removed. The viscous liquid was then redissolved in minimum volume of hot acetonitrile (70 mL) and cooled to room temperature. Cold diethyl ether was added until the solution remained cloudy, and the mixture was cooled in a freezer for 15 h. The recrystallisation product was isolated via vacuum filtration under flow of inert gas, quickly as it soon became a viscous liquid once its temperature increased. The recrystallisation stage was repeated and the final product was dried under vacuum (10⁻² mbar, 24 h) giving [meta-xylene-(C₈Im)₂]Cl₂ (3.98 g, 11.2 mmol, 27%). ¹H NMR (400 MHz, DMSO) δ 9.75 (d, J = 1.7 Hz, 2H), 7.95 (t, J = 1.8 Hz, 2H), 7.86 (t, J = 1.8 Hz, 2H), 7.73 (s, 1H), 7.45 (d, J = 1.4 Hz, 3H), 5.48 (s, 4H), 4.20 (t, J = 7.3 Hz, 4H), 1.80 (p, J = 7.2 Hz, 4H), 1.24 (dq, J = 11.7, 6.0 Hz, 20H), 0.84 (t, J = 6.8 Hz, 6H). ¹³C NMR (101 MHz, DMSO) δ 136.46, 135.72, 129.60, 128.77, 128.60, 122.69, 122.55, 64.91, 51.50, 48.93, 48.53, 31.13, 30.69, 29.29, 28.49, 28.31, 25.54, 22.04, 15.16, 13.93. **MS (ESI +)** (m/z (%)): 232.1941 (100), 232.6956 (35.9), 233.1970 (6.2).

1,3-Bis-(N-octylimidazolium-1-yl)xylene Bis(trifluoromethylsulfonyl)imide, [m-xyl-(C₈Im)₂][NTf₂]₂

LiNTf₂ (3.51 g, 12.2 mmol) was dissolved in deionised water (20 mL) and added to [meta-xyl-(C₈Im)₂]Cl₂ (2.73 g, 5.10 mmol) in deionised water (20 mL). The reaction mixture was stirred vigorously at room temperature for 24 h leading to the formation of a colourless viscous liquid that was insoluble in the H₂O. The IL product was extracted using dichloromethane (~2 mL) and washed repeatedly with pure H₂O until a silver nitrate test on the aqueous layer no longer indicated the presence of Cl ions. The solvent was removed *in vacuo* and the IL was dried to remove water (< 10⁻¹, 60 °C, 24 h) to yield the pure product, [m-xyl-(C₈Im)₂][NTf₂]₂ (2.96 g, 3.97 mmol, 77.8%). ¹H NMR (400 MHz, DMSO) δ 9.26 (d, J = 1.7 Hz, 2H), 7.83 (t, J = 1.8 Hz, 2H), 7.76 (t, J = 1.8 Hz, 2H), 7.53 – 7.44 (m, 2H), 7.38 (dd, J = 7.4, 1.8 Hz, 2H), 5.42 (s, 4H), 4.16 (t, J = 7.3 Hz, 4H), 1.79 (p, J = 7.3 Hz, 4H), 1.31 – 1.19 (m, 20H), 0.89 – 0.81 (m, 6H). ¹³C NMR (101 MHz, DMSO) δ 136.20, 135.53, 129.80, 128.50, 128.25, (NTf₂: 124.28, 121.08, 117.88, 114.68), 122.85, 122.58, 51.70, 49.02, 31.13, 29.28, 28.47, 28.30, 25.51, 22.04, 13.90.

Trioctylammonium bis(2-ethylhexyl)phosphate, [N_{888H}][DEHP]

Synthesised following the neutralisation reaction method outlined in the literature.⁹⁴ Bis(2-ethylhexyl) phosphate (97% purity) was purchased from Sigma Aldrich. Tri-n-octylamine (97% purity) was purchased from Thermo Scientific.

Di(2-ethylhexyl) phosphate (HDEHP) (4.56 g, 14.14 mmol) was added dropwise to trioctylamine (5.00 g, 14.14 mmol) with vigorous stirring. The mixture was reacted at room temperature for 2 h, yielding [N_{888H}][DEHP] as a viscous colourless liquid (9.56 g, 14.14 mmol, 100%). ¹H NMR (400 MHz, CDCl₃) δ 13.44 (s, 1H, NH), 3.71 (h, J = 4.9 Hz, 4H, 2OCH₂), 3.06 – 2.65 (t, 6H, 3NCH₂), 1.66 (m, 6H, 3CH₂), 1.50 (m, 2H, 2CH), 1.34 – 1.17 (m, 46H, 23CH₂), 0.97 – 0.66 (m, 21H, 7CH₃). ¹³C NMR (101 MHz, CDCl₃) δ 67.76 (d, J = 6.0 Hz), 51.78, 40.50 (d, J = 8.0 Hz), 31.79, 30.23, 29.31 – 29.11 (m), 27.08, 23.35 (d, J = 23.3 Hz), 22.67, 14.18 (d, J = 8.3 Hz), 11.07. **MS (ESI +)** (m/z (%)): 354.4101 (100), 355.4133 (26.1).

Trihexyltetradecylphosphonium bis(2-ethylhexyl)phosphate, [P₆₆₆₁₄][DEHP] (>98% purity)

Purchased from Iolitec as opposed to synthesising in house due to its affordability and guaranteed high purity, which was confirmed via NMR analysis. ¹H NMR (400 MHz, DMSO) δ 3.47 – 3.36 (m, 4H), 2.25 – 2.12 (m, 8H), 1.51 – 1.16 (m, 62H), 0.90 – 0.79 (m, 24H). ¹³C NMR (101 MHz, DMSO) δ 65.73, 65.67, 40.08, 40.00, 31.29, 30.81, 30.41, 30.06, 29.99, 29.91, 29.84, 29.69, 29.06, 29.04, 29.00, 28.95, 28.70, 28.65, 28.63, 28.10, 23.23, 22.64, 22.09, 21.91, 21.82, 20.57, 20.53, 17.72, 17.63, 17.25, 13.98, 13.93, 13.89, 13.84, 10.94.

6.2 Analysis

Viscometer

Dynamic viscosity (μ), kinematic viscosity (ν) and density (ρ) of the RTILs and the base oil mixtures were recorded using an Anton Paar SVM 3000 Viscometer. Measurements were taken at 10 °C temperature intervals from 20 – 100 °C using a sample size of at least 3 mL. Samples were dried at $\sim 10^{-2}$ mbar pressure at 50 - 70 °C for at least 24 h prior to viscometer data collection. Due to time restraints, it was not possible to repeat experiments for all samples. However, reproducibility analysis was conducted using $[C_4(C_{1Im})][NTf_2]$ and, as anticipated, process related issues such as variabilities in water content had a greater impact than the reported error of the instrument (0.1% for viscosity, 0.0002 g/cm³ density). At 20 °C, $[C_4(C_{1Im})][NTf_2]$ was calculated to have an average dynamic viscosity of 63.2145 mPa·s \pm 0.30%, kinematic viscosity of 43.9195 mm²/s \pm 0.27%, and density of 1.4394 \pm 0.03% g/cm³. The deviation in dynamic viscosity ranged from 0.16% – 0.30%, kinematic viscosity ranged from 0.15% - 1.12%, and density ranged from 0.01% - 0.03%. It was found that deviations between the two experiments were more significant at lower temperatures and the data sets converged at higher temperatures. In depth error analysis of $[C_4(C_{1Im})][NTf_2]$ can be found in the appendix, Table 8-Table 10.

Differential Scanning Calorimetry (DSC)

DSC analysis was performed using a TA Instruments Discovery DSC with Tzero aluminium hermetic pans using a sample mass of 3-5 mg. Pinholes were made in the hermetic platinum lids to allow for the removal of any moisture present during a pre-experimental drying stage which took place at 100 °C for 45 min. The experimental procedure involved repeated cooling and heating temperature cycles, beginning by ramping down to -80 °C and then up to 150 °C. Initially a 20 °C/min cycle occurred followed by a 10 °C/min cycle, which was repeated, and finally a 5 °C/min cycle. At the lower and upper temperature limits the sample was held isothermally for 1 min to ensure thermal stabilisation of the instrument was achieved.

Quasi-isothermal Modulated DSC (QiMDSC) analysis was performed using the same instrument and pans, however with a much larger sample mass of 8-13 mg. For neat ILs, the pinhole pre-experimental drying method was employed again, however when studying the samples containing PAO hydrocarbon oils, a drying stage was not conducted due to concerns of vaporisation and contamination of the instrument (as well as compromised data). The $[P_{66614}][DEHP]$ and $[N_{888H}][DEHP]$ ILs were extensively dried under reduced pressure ($<10^{-1}$, 24 h) at 50 °C and the experiments were repeated without the drying stage inside the instrument to allow for better comparability to the base oil mixtures. The QiMDSC experiment involved measuring samples isothermally at 10 °C increments (beginning at 20 °C and terminating at 120 °C) whilst temperature was modulated \pm 1 °C. Heat flow measured during this enabled normalised reversing heat capacity, C_p , at each temperature to be obtained in J/(g·°C).

Thermogravimetric Analysis (TGA)

TGA was measured on a TA Instruments Discovery TGA 550 using high temperature (HT) platinum pans with a 50 mL/min flow of inert gas (N₂). The pans were cleaned by heating thoroughly with a propane torch in air, oxidising any decomposition residues from previous use. The standard method used for ILs involved an initial drying stage where the sample was kept isothermally at 100 °C for 20 min. This aimed to remove any water that was absorbed while the samples were on the autosampler

(up to 6hr). After this, the sample was heated to 600 °C at a rate of 10 °C/min to give the thermal stability profiles of the samples with increasing temperature.

Melting Point Apparatus

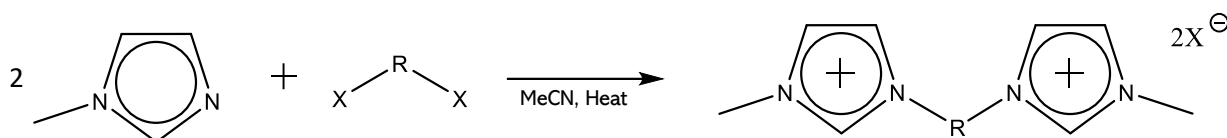
Melting point determination of the solid bromide salts was recorded using a Stuart SMP20 capillary tube melting point analysis instrument with a 1 °C/min heating rate. Samples were measured in air on the benchtop.

Karl Fisher Titration

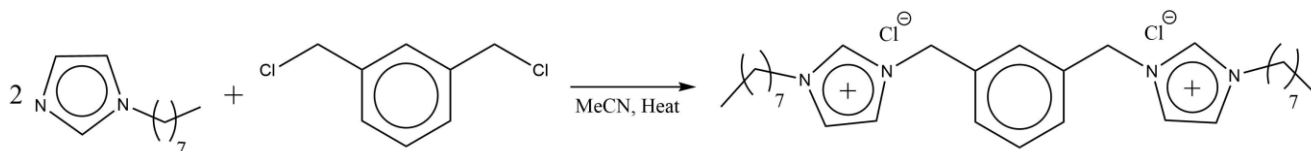
Karl Fisher Titration was used to measure the water content of the ILs after drying at increased temperature and reduced pressure. The method involved syringing ~10 mL of IL (2-5 mL in cases where a low IL yield was obtained) from the drying vessel, under an inert Ar atmosphere, and injecting this into the titration electrolyte fluid. Mass measurements were taken before and after the injection of the IL and were imputed into the machine to calculate the water content in ppm. In many cases, results were given where H₂O was found to be <100 µg. The titration instrument manufacturer reports that titration results with moisture content below this value cannot be considered reliable, and that larger sample sizes would be required. This however was not possible in many cases since Karl Fischer titration is a destructive method and large quantities of valuable ILs could not be afforded to be used in this capacity.

7. Results and Discussion

A range of IL species were synthesised and studied experimentally to give insight into the overall suitability of ILs for use in this capacity. $[C_4(C_1Im)][NTf_2]_2$ was initially synthesised as a species that would act as a good indicator that the physical property experiments executed were accurate and comparable to previous studies. $[C_4(C_1Im)]^+$ is one of the most widely studied cations in IL literature and therefore there is extensive data on its physical properties.⁹⁵ However, with all other ILs in this investigation, the literature provided a less wholistic overview of their properties – especially species such as $[C_{10}(C_1Pyrr)_2][NTf_2]_2$ and $[m\text{-xyl}-(C_8Im)_2][NTf_2]_2$ which appear to be novel. For this reason, the intention of this investigation was to fill some of the gaps in the thermophysical data of a selection of promising IL species to provide a well-rounded assessment of their appropriateness for use as a new class of lubricant and thermal fluids in EVs.



Scheme 1 - General synthesis of 1-methyl-3-alkylimidazolium dicationic IL (where $X = Br$ and $R = (CH_2)_n$).



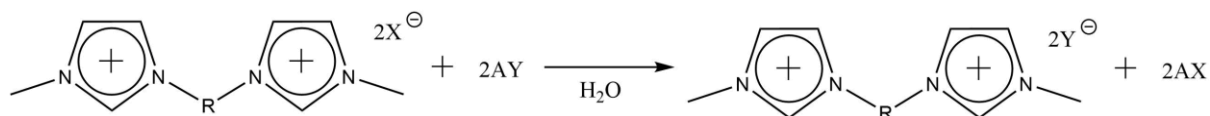
Scheme 2 – Synthesis of $[m\text{-xyl}-(C_8Im)_2]Cl_2$ via a nucleophilic substitution reaction.

Dicationic imidazolium bromide salts were synthesised via the nucleophilic substitution reaction outlined in Scheme 1. It was necessary to use an excess of methylimidazole to ensure that both substitutions of the dibromo-alkyl chain were made, as mono-substituted cations would lead to impurities which are difficult to remove from the product due to having a similar structure and solubility and being essentially involatile, making separation via vacuum unfeasible. As well as this, reactions were refluxed to provide sufficient energy to promote lots of collisions and the timescale of the reactions were relatively long compared to typical nucleophilic substitution synthesis.

Scheme 2. shows the more complex nucleophilic substitution of N-octylimidazole with m-xylylene dichloride to give $[m\text{-xyl}-(C_8Im)_2]Cl_2$. The dichloride reactant was used as opposed to a dibromide reactant purely due to ease of sourcing and cost. The reaction was run for a further 24h at a higher temperature than the method described in the literature which used a bromide reagent because the substitution reaction took longer to complete due to stronger C-Cl bonds. This IL was synthesised to observe the impact on the physical properties of adding benzene functionality to the bridging chain.

Reactions were monitored with 1H NMR, by taking an aliquot of the reaction mixture after it was expected that it would be completed based on similar synthesis in the literature. This was relatively effective, however the acetonitrile solvent and 1-methylimidazole excess starting material complicated the spectra, making it difficult to determine the completion of a reaction in some cases. However, monosubstituted species were often identifiable by smaller signals at a slightly lower ppm than peaks from the desired product. For the imidazolium species it was easiest to see these monocation peaks on the isolated singlet often found in the range 9.1-9.8 ppm, where the proton between the nitrogen atoms in the imidazole ring is significantly chemical shifted. The two triplet

signals usually found at 7.7–7.8 ppm also had slightly upfield tail peaks when the reaction hadn't been driven to completion.



Scheme 3 - General synthesis of anion exchange of dicationic imidazolium IL via metathesis reaction (Where $R = (CH_2)_n$, $X = Br/Cl$ and $Y = [NTf_2]^-$)

The desired $[NTf_2]^-$ containing DILs were synthesised from their halogen salt precursors via the anion exchange metathesis reaction outline in Scheme 3. This was carried out in H_2O which helped to ensure any excess $LiNTf_2$ was dissolved in the water rather than being removed with the insoluble ILs. Using H_2O as a solvent and carrying out the metathesis at room temperature ensures compliance with green chemistry practices. For many of the species multiple washes were required to completely remove the $LiNTf_2$ and any halogen salts. Multiple hours were left between each wash to ensure the complete separation of the layers.

7.1. DSC Analysis of Neat ILs

Thermophysical properties such as phase-change behaviour (i.e. glass transitions, melting points) and heat capacity were collected to provide an in-depth understanding of the behaviour of the ILs over a wide temperature range. This analysis is crucial in determining the liquid range of the ILs, and therefore review their suitability as high-performance fluids in EV transmissions and e-motors. A wide liquid range is crucial in this application as internal temperatures can fluctuate significantly when the vehicle is in standby or being driven, as well as being influenced by the conditions of the external environment. Consequently, the fluids must operate effectively, with immediate effect, when the vehicle is powered up. This may mean that the fluids are at atmospheric temperatures in these situations, which depending on the weather conditions, can be far below $0\text{ }^\circ\text{C}$. If fluids are in a solid or glass state at these temperatures, significant mechanical damage may occur as lubricants resist bearing motion, and possibly also contribute to wear of moving parts.

IL	T_g (°C)	T_m (°C)	$C_p(20^\circ\text{C})$ (J/mol·°C)	$C_p(120-20^\circ\text{C})$ (J/mol·°C)	$T_{D(\text{onset})}$ (°C)	$T_{D(1\%)}$ (°C)
[C ₄ (C ₁ Im)]Br	-48.1 -50.0 ⁷²	73.7 ^b	-	-	274.5	226.3
[C ₄ (C ₁ Im)][NTf ₂] ₂	-87.2 ⁹⁶ -87.0 ⁹⁷ -86.0 ⁷²	-	449.8 ± 0.5	37.0 ± 0.7	408.4	322.5
[C ₁₀ (C ₁ Im) ₂]Br ₂	0.3 ± 0.4	145.6 ^b	-	-	280.8	237.8
[C ₁₀ (C ₁ Im) ₂][NTf ₂] ₂	-61.5 ± 0.3 -57.4 ± 0.7 ⁹⁸	-	614.6 ± 0.4	43.7 ± 0.5	435.0 416.3 ⁹⁸	385.5
[C ₁₀ (C ₁ Pyrr) ₂]Br ₂	31.8 ^a 32.6 ^b	211.3	-	-	267.1	254.7
[C ₁₀ (C ₁ Pyrr) ₂][NTf ₂] ₂	-54.3 ± 0.1	-	745.7 ± 0.4	66.2 ± 0.7	419.6	386.9
[C ₁₀ (C ₈ Im) ₂]Br ₂	-36.3 ± 1.7	93.0 ^b	-	-	265.6	225.9
[m-xyl-(C ₈ Im) ₂]Cl ₂	-	-	-	-	247.7	196.8
[m-xyl-(C ₈ Im) ₂][NTf ₂] ₂	-51.6	-	870.1 ± 0.5	92.8 ± 1.0	382.5	287.5
[N _{888H}][DEHP]	-	-	1219.1 ± 0.8	178.9 ± 1.1	225.3	164.3
[P ₆₆₆₁₄][DEHP]	-	-	1629.5 ± 1.0	129.1 ± 1.6	281.4 298.0 ⁹⁹	191.1

Table 2 - Thermal analysis parameters from DSC and TGA experiments - the glass transition temperature, T_g , melting point, T_m , heat capacity at 20 °C, $C_{p(20^\circ\text{C})}$, heat capacity range from 20 to 120 °C, $C_{p(20-120^\circ\text{C})}$, thermal degradation onset temperature, $T_{D(\text{onset})}$, 1% thermal degradation temperature, $T_{D(1\%)}$. **a** – obtained from DSC with a 10°C/min heating rate, however an atypical glass transition signature was observed, **b** – obtained using capillary melting point apparatus.

Melting points of the ILs were determined using DSC where possible, however, due to the action of drying samples at 100 °C for 20 min and then supercooling to -80 °C at 20 °C/min, in most cases an amorphous glass state was formed which did not display conventional melting and crystallisation patterns. Imidazolium ILs tend to exhibit glass transitions as opposed to defined melting and crystallisation, therefore it is only by cooling very slowly that crystals are formed. These crystals may subsequently melt like typical organic species, giving a distinct endothermic peak in the DSC thermogram, or they can transition from the solid crystalline state to an amorphous glass. The melting points of the other bromide salts were determined using capillary melting point apparatus and were therefore established visually.

The property of melting point is directly related to the strength of the crystal lattice of a solid structure.¹⁰⁰ Lattice strength is influenced by the intermolecular forces, molecular symmetry and conformational degrees of freedom of a molecule.¹⁰¹ It is essential for ILs to have low melting points (<-20 °C) to be appropriate for use in EVs, since lubricating properties are only achievable in the liquid state, and the vehicles must be fully operational in cold temperatures as well as warmer climates.

As cited in the literature, anion selection has a large influence upon the melting points of ILs, with the widely studied [NTf₂]⁻ anion often yielding the lowest temperature liquid ranges.⁶² ILs with this anion prefer the amorphous glass state due to the anion being structured so that negative charge is delocalised along the S–N–S centre, with additional shielding provided by the non-charge carrying sulfonyl oxygens and trifluoromethane groups. This results in a charge diffuse and weakly coordinating anion, which is weakly attracted to cation species leading the IL to transition states with no mesomorphism, to form isotropic liquids.¹⁰²

All the ILs in this study with the [NTf₂]⁻ anion were liquid at room temperature and displayed glass transitions in DSC analysis. The exception was [C₄(C₁Im)] [NTf₂] in which other studies have reported a glass transition that occurs at the lower limit of the range of the RCS90 chiller used in this study (transition in the range -86 °C to -87 °C).^{96,97} Therefore, in the data collected the transition signal was most likely hidden due to an overlap with the “start-up hook” - the initial large dip usually found at the beginning of a DSC thermogram which occurs as the system approaches equilibrium temperature.¹⁰³ Glass transitions were recorded as the midpoint of the change in heat flow, as is standard practice in the literature. [C₁₀(C₁Im)₂] [NTf₂]₂ had a glass transition that occurred 61 °C lower than its bromide equivalent (-61.5 ± 0.3 °C, 0.3 ± 0.4 °C respectively). A melting point could also be determined for the bromide salt at 145.6 °C using capillary tube melting point apparatus, showing the temperature of the liquid melt from the solid crystal which was obtained through slower recrystallisation methods. In this case, the bromide salt showed fluid behaviour at a temperature 207 °C above the [NTf₂]⁻ equivalent. Whereas [C₁₀(C₁Pyrr)₂] [NTf₂]₂ had a glass transition 86.6 ± 0.4 °C lower (31.8 °C) and was liquid 265.6 ± 0.1 °C lower. In fact, all ILs with the [NTf₂]⁻ anion displayed glass transitions at temperatures <-50 °C, and this was the only transition observed from the liquid state, making them excellent candidates for use in low temperature environments.

Aside from anion selection, melting point is also strongly influenced by the structure of the cation. For example, imidazolium species have been known to have lower melting points than structurally equivalent pyrrolidinium species. This is confirmed in Table 2. as [C₁₀(C₁Pyrr)₂]Br₂ was recorded as having a melting point 65.7 °C higher than [C₁₀(C₁Im)₂]Br₂. Numerous studies have shown geminal dicationic ILs to have higher melting points than monocationic ILs with similar alkyl substituents. In part, this is due to increased symmetry and therefore increased order in the arrangement of the molecules – Carnelly’s rule.¹⁰⁴ As seen in Table 2., dications with halide anions were observed to have higher melting points than [C₄(C₁Im)]Br (in the case of [C₁₀(C₁Im)₂]Br₂ an increase of approximately 2x was observed). In addition, dications with long spacer alkyl chains between the two cationic moieties tend to be liquid at room temperature due to their high conformational degrees of freedom available from the rotatable Sp³ centres. Extending alkyl chains on the 1 position of the imidazolium ring from a methyl to octyl hydrocarbon substituent was shown to decrease the melting point of the imidazolium bromide IL. The [m-xyI-(C₈Im)₂]²⁺ ILs were both liquid at room temperature and didn’t show defined crystallisation at reduced temperatures. This can likely be attributed to the long alkyl chains in the cation, leading to difficulties in packing to form an ordered crystal lattice.

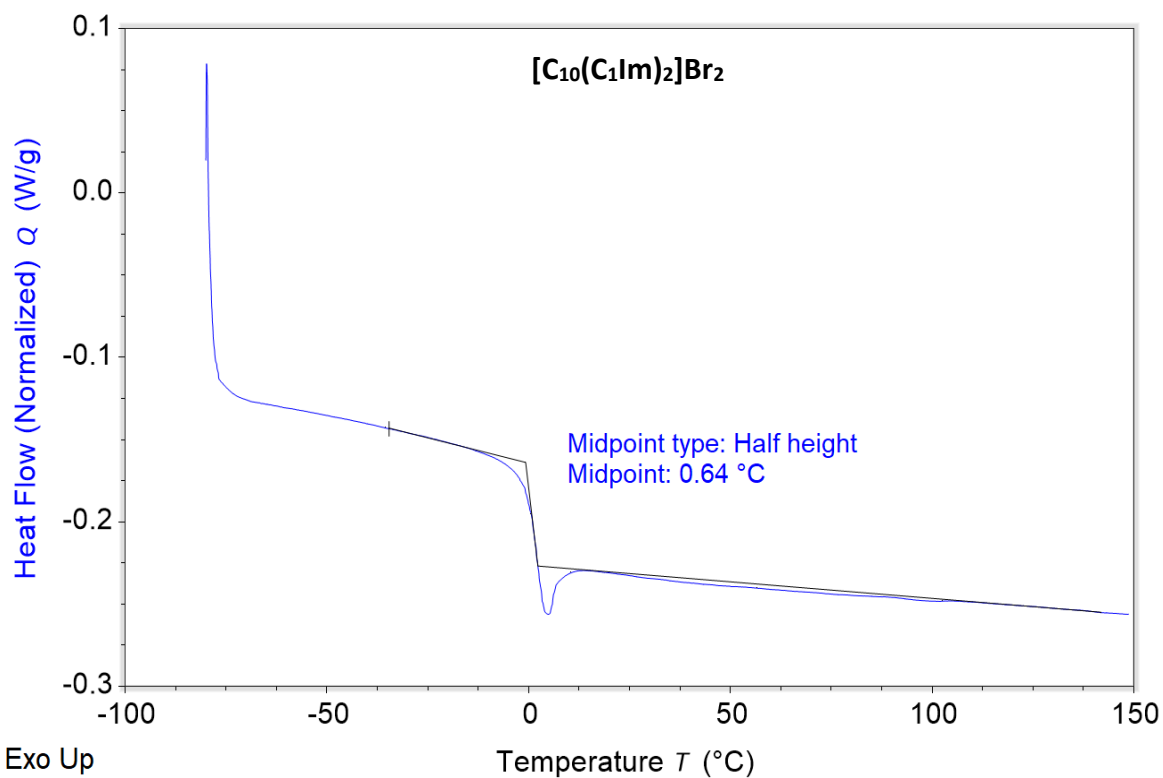


Figure 2 - DSC thermogram of $[C_{10}(C_1Im)_2] Br_2$ showing a glass transition during $10\text{ }^\circ\text{C}/\text{min}$ heating.

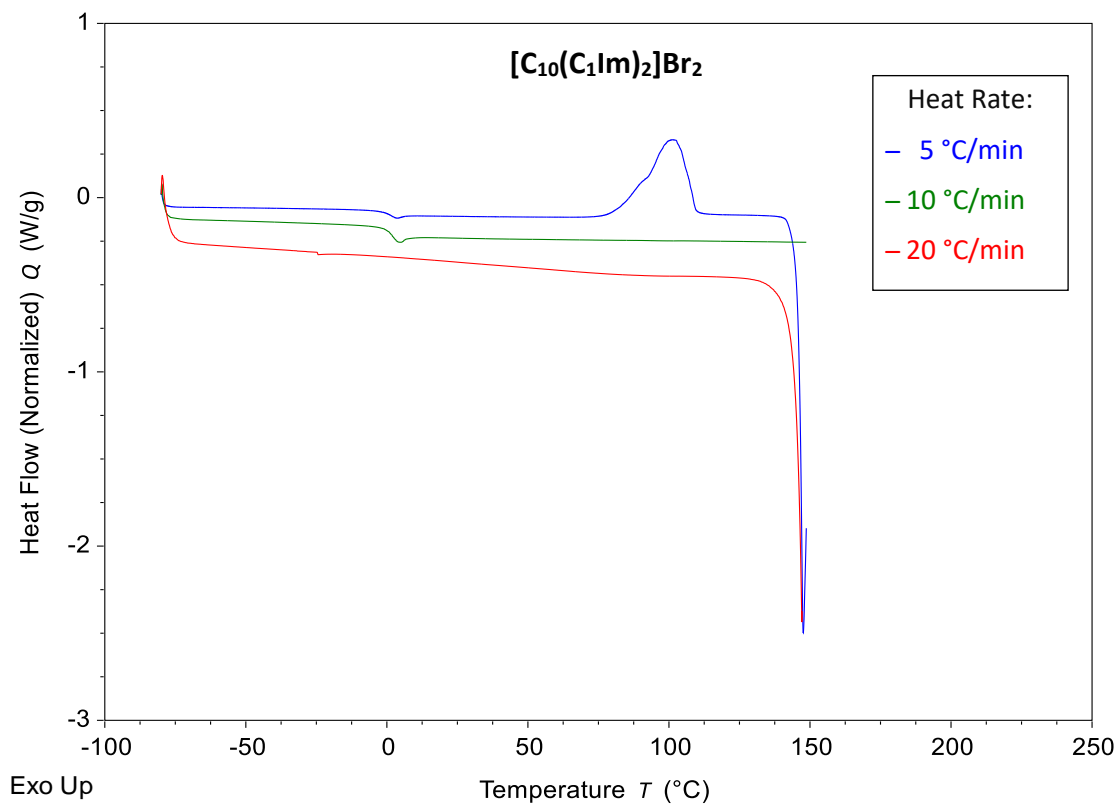


Figure 3 - DSC thermogram of $[C_{10}(C_1Im)_2] Br_2$ at different heating rates from $-80\text{ }^\circ\text{C}$ to $150\text{ }^\circ\text{C}$.

Figure 2. shows a typical glass transition for the class of ILs studied in this investigation. Crystalline solid samples such as this one likely melted during the 45 min, 100 °C isothermal drying procedure, and during cooling, transitioned to a glass without displaying an exothermic signal such as a conventional crystallisation peak. Glass transitions occurred upon heating and often include enthalpy relaxation due to the molecules being locked into high energy confirmations upon rapid cooling. This energy is released when the glass transition occurs. Endothermic enthalpy relaxation peaks occur at the end of the glass transition step and often had a peak area (enthalpy) of about 1 J/g. Different behaviour was observed at different heating and cooling rates. An example of this is shown in Figure 3. where a broad exothermic signal was observed for the $[C_{10}(C_1Im)_2][NTf_2]_2$ sample with an onset temperature of 80.3 °C and a peak temperature of 101.2 °C, only occurring during the 5 °C/min heating rate experiment and not at the slower rates.

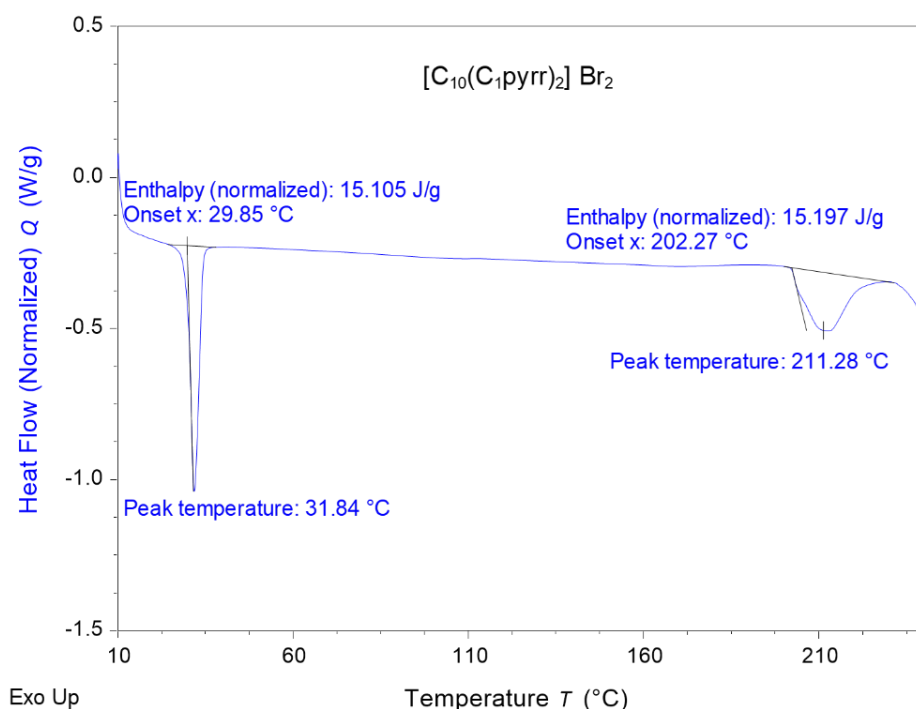


Figure 4 - DSC thermogram of $[C_{10}(C_1Pyrr)_2] Br_2$ at a 10 °C/min heating rate.

Figure 4. shows the $[C_{10}(C_1Pyrr)_2]Br_2$ IL which displays a more complex melting behaviour – an initial melt is shown at 31.8 °C followed by a much broader transition at 211.3 °C. It may be the case that a solid-solid transition is occurring at 211.3 °C since such a broad signature is displayed, however, more analysis is required in future work to conform this.

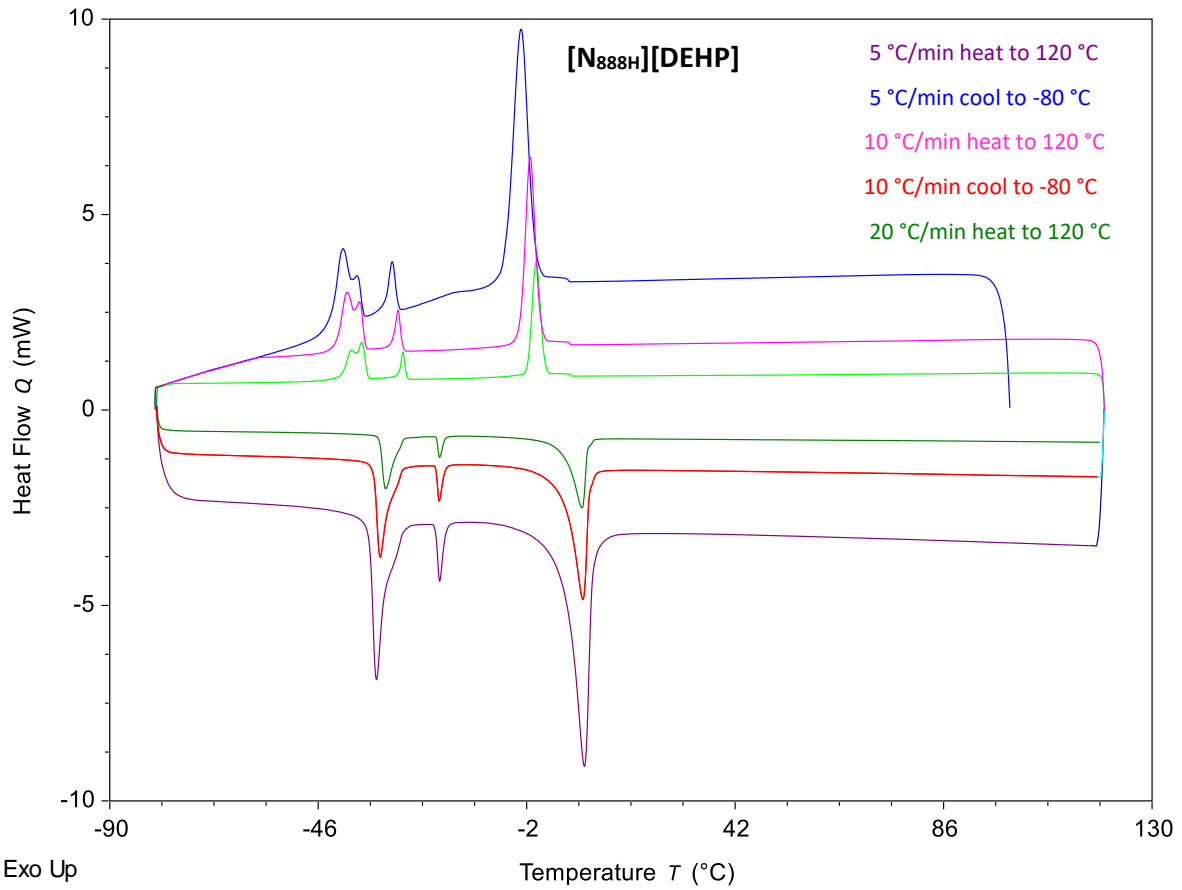


Figure 5- DSC thermogram of [N_{888H}][DEHP] heating and cooling cycles at a range of different rates.

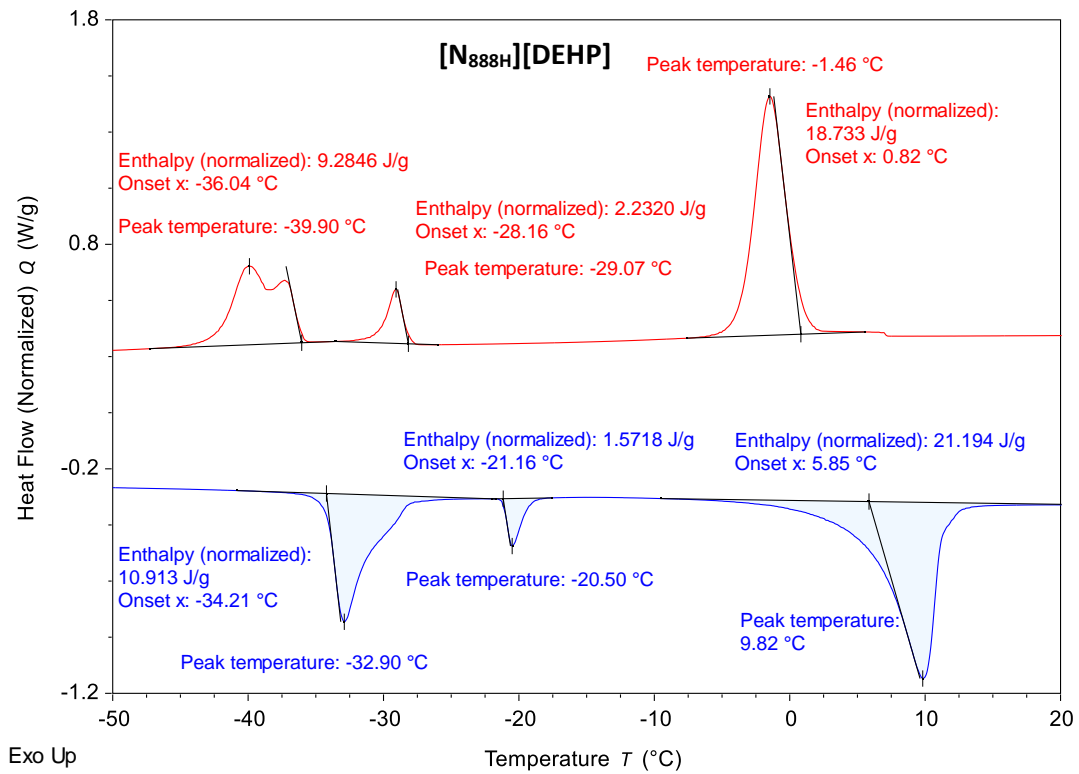


Figure 6 - DSC thermogram of [N_{888H}][DEHP] at 10 °C/min rate of heating (blue plot) and cooling (red plot). Annotated with peak temperatures of each transition and enthalpy, determined from the peak integration.

[N_{888H}][DEHP] gave the most complex DSC thermogram, displaying three distinct endothermic signals during heating and three exothermic transitions during cooling. This indicates that three individual components of the IL transition independently at different temperatures, contrasting the rest of the ILs studied. The peak observed at 9.8 °C during heating is likely a partially crystalline liquid melt – the broadness of the peak is a result of the size distribution of the crystallites.¹⁰⁵ It should also be considered that this is an acid-base pair that behaves in equilibrium. Hence, the peaks could originate from the original acid and base if the temperature shifts the equilibrium. This can be determined in future research. Regardless, the highest temperature peaks are a good indication of the lowest operating temperature, since even partial crystallisation with solid crystals suspended in a liquid media would disrupt the lubricating and heat transfer abilities, making it less effective.

7.2. Thermal Stability of Neat ILs

Thermal stability measurements were an essential aspect of this project as they are used to determine the upper temperature range of use of the ILs. To be suitable for application in EV motors, the ILs must be stable at least up to 180 °C which is the maximum temperature of the copper coils.²⁷

As seen in Table 2., the 1% mass loss temperature, $T_{d(1\%)}$, was determined from the TGA thermograms, in addition to the thermal degradation onset temperature, T_d . This is because scan rate has a significant impact on the apparent thermal degradation temperature. Kosmulski *et al.* (2004) stated that a decrease in scan rate by a factor of 10 resulted in a dramatic shift in the apparent decomposition temperature of ILs.¹⁰⁶ In application in EVs as e-motor lubricants and thermal fluids, the ILs would be subjected to prolonged periods of high temperatures and therefore must be stable to extended heating. $T_{d(1\%)}$ is a parameter that gives a good indication of this whilst also enabling the collection of the thermal degradation profile over a wide temperature range to analyse if decomposition is a single or multi-step process for these ILs. An alternative method of determining thermal stability is to heat isothermally at high temperature for extended periods. However, the T_d must be known in order to select an appropriate isothermal temperature (typically 10% lower than T_d) and the method is highly time demanding, especially when studying a large number of samples. Therefore, this additional data should be collected in future work.

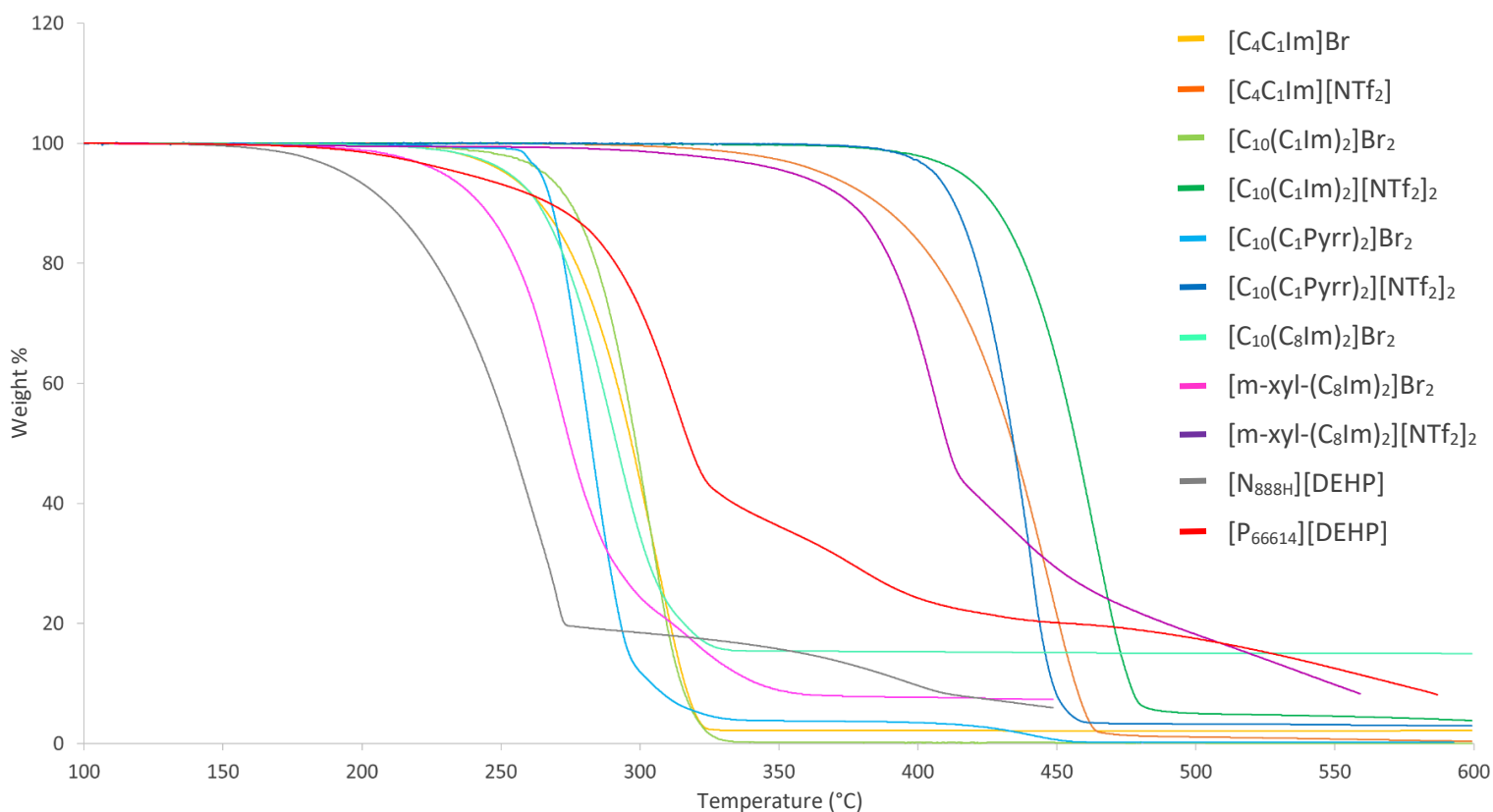


Figure 7 - Thermal degradation of a range of ILs determined via TGA with a 10 °C/min heating rate under N₂ gas flow.

Figure 7. shows the thermal degradation profiles of all the neat IL species in this experimental study. It can be observed that there is a clear gain in thermodynamic stability achieved from the transition from a monocationic IL to a geminal DIL. For instance, an increase in T_d of 6.3 °C was recorded between [C₄(C₁Im)]Br and [C₁₀(C₁Im)₂]Br₂ and an increase of 26.6 °C was recorded between [C₄(C₁Im)][NTf₂]₂ and [C₁₀(C₁Im)₂][NTf₂]₂. This supports the findings of Anderson et al. (2005) who observed similar gains in thermodynamic stability when comparing geminal ILs to traditional monocationic ILs.⁶²

As anticipated, anion selection was observed to be the variable that resulted in the most notable increase in thermal stability, with the [NTf₂]⁻ anion significantly increasing the thermal stability of all IL species from their Br or Cl precursors. On average, ILs containing the [NTf₂]⁻ anion had a T_d that was 143.9 ± 9.5 °C higher than their halide anion equivalents and an average $T_{D(1\%)}$ increase of 116.7 ± 24.0 °C. This phenomenon has been widely observed in the literature and has been attributed to the low nucleophilicity of the anion which is the result of the highly electron withdrawing CF₃ groups spreading the negative charge from the N-SO₂ groups across the whole anion.¹⁰⁷ The larger molecular weight of the anion also has a positive influence on its stability.¹⁰⁸

[C₁₀(C₁Im)₂][NTf₂]₂ was found to be the most thermally stable in terms of onset temperature, whereas [C₁₀(C₁Pyrr)₂][NTf₂]₂ showed higher stability when considering 1% mass loss temperature. Both DILs are large geminal dicationic species paired with the [NTf₂]⁻ anion and therefore the positive stability effects of the previously discussed variables were compounded. [m-xyI-(C₈Im)₂][NTf₂]₂ was less stable compared to the other ILs with [NTf₂]⁻, perhaps because of the smaller bridging chain and exposed long octyl substituents on the imidazole groups which are often the area of ILs most sensitive to thermal degradation.¹⁰⁹

Most ILs left a decomposition residue, shown by many of the plots in Figure 7. not levelling off at 0% weight – for instance $[C_{10}(C_8Im)_2]Br_2$ left 15% of its initial mass as residue which remained throughout the temperature range. However, if these experiments were run in O_2 as opposed to inert N_2 , the samples would most likely fully oxidise without leaving a residue. In application in machinery, decomposition of any degree is undesirable and could cause mechanical issues since the materials would no longer be able to effectively carry out their intended functions. The formation of chemical by-products could also potentially damage internal parts through reactivity. This is a further reason for intensive corrosion and reactivity testing of the ILs to be carried out with the materials present in EV parts to establish their suitability as lubricants and heat transfer fluids in these environments.

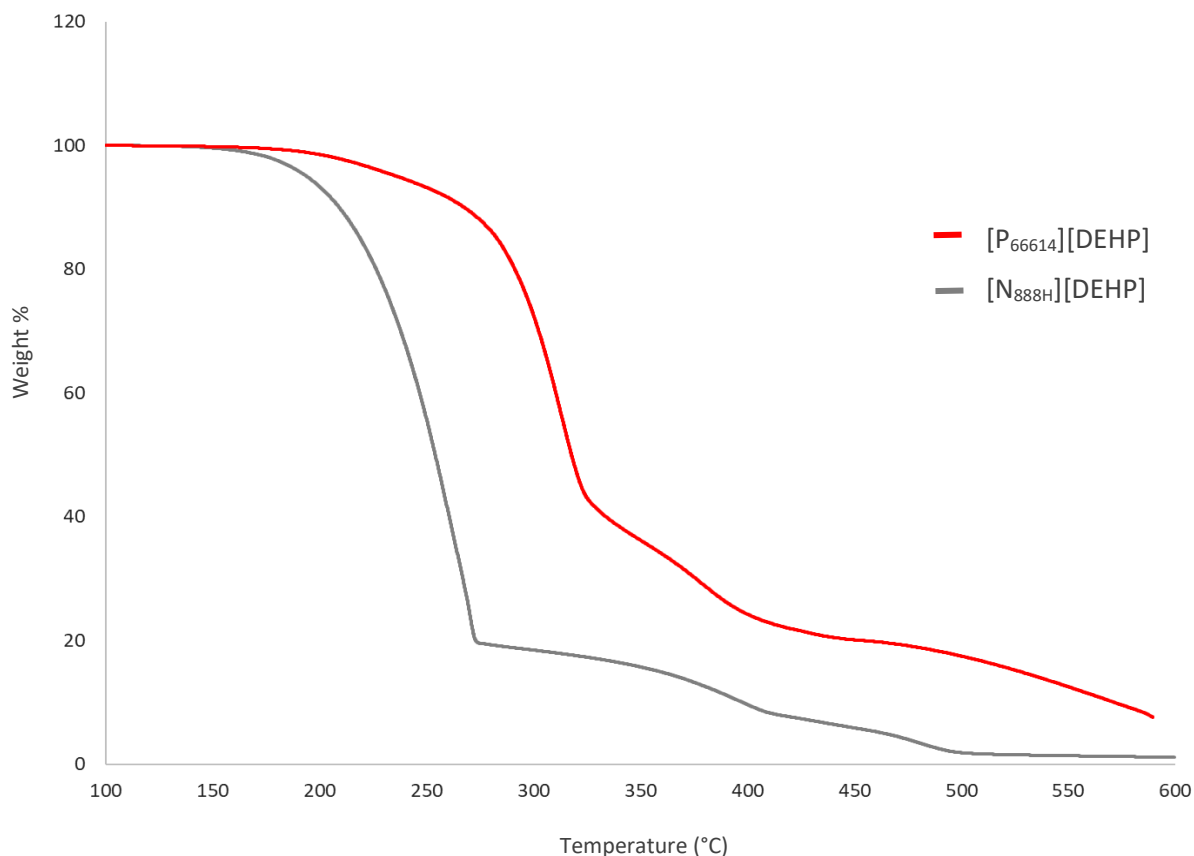


Figure 8 - Thermal stability of $[N_{888H}][DEHP]$ and $[P_{66614}][DEHP]$.

$[N_{888H}][DEHP]$ was the least thermally stable IL in this investigation, with a $T_{d(1\%)}$ of just 164.3 °C. $[N_{888H}][DEHP]$ and $[P_{66614}][DEHP]$ indicated a different decomposition mechanism through their TGA thermograms which can be seen in isolation in Figure 8. For both ILs, an initial mass loss curve was recorded followed by a less defined, broad peak at higher temperatures. This behaviour has been observed in previous studies and linked to the increased reactivity of the nucleophilic phosphate anion which causes alkyl groups on the cation to pyrolyze at temperatures at and above 300 °C.⁹⁹

7.3. Heat Capacity (C_p) of Neat ILs

Heat capacity, C_p , is a measurable physical quantity that characterises the amount of heat required to change the temperature of a molecule/compound by a given amount. It is therefore more favourable that ILs have a higher C_p when considering their use as thermal management fluids as a higher C_p results in more energy being captured by the IL, thus reducing the temperature of the heat source. Therefore, investigating this metric identifies which of the ILs in this study would likely be the most effective as thermal fluids, as these species display the highest C_p values.

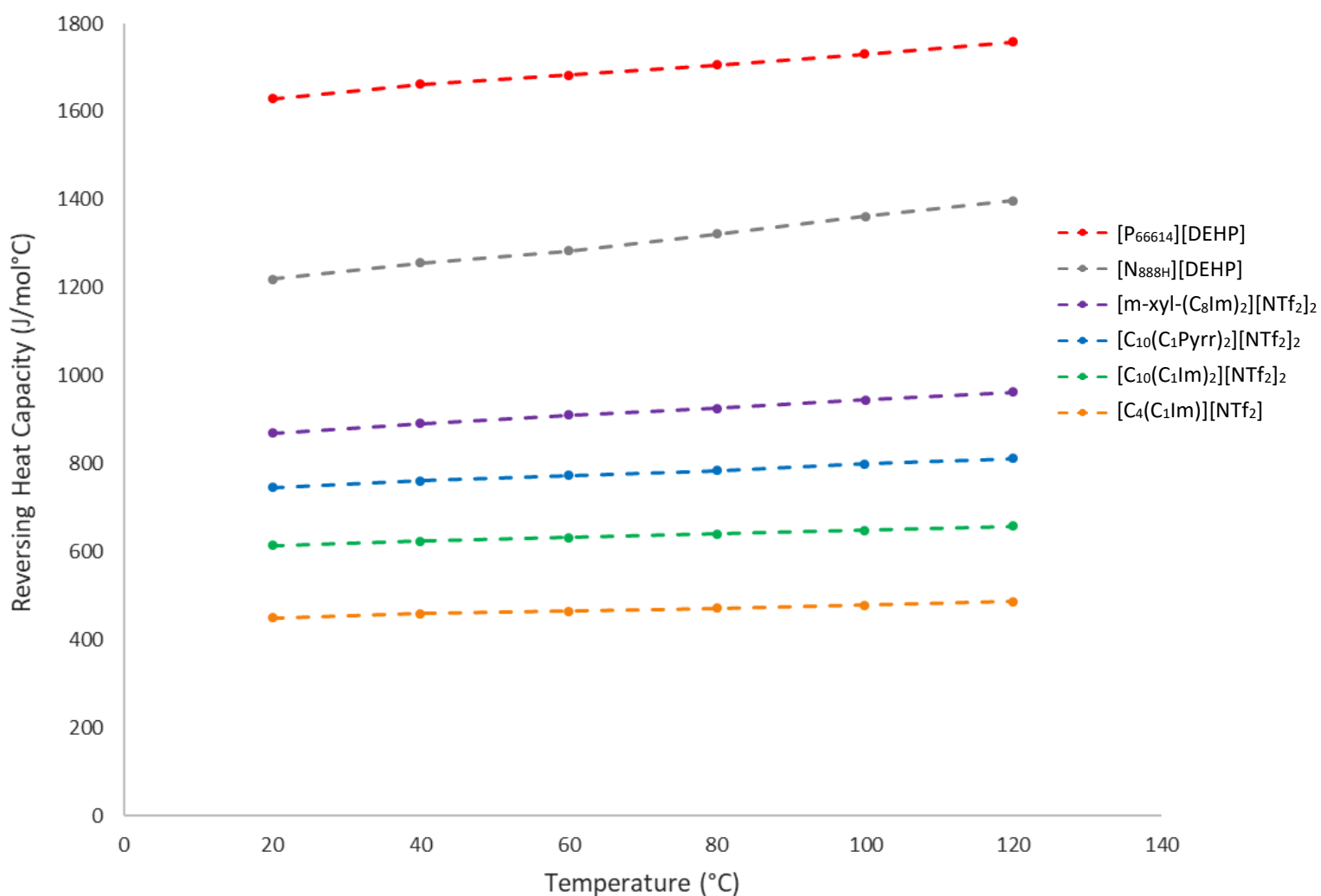


Figure 9 - The reversing heat capacities of a range of ILs recorded with QiMDSC at 20 °C intervals.

As seen in Figure 9., the C_p data obtained in this investigation largely fits the generally observed relationship in which C_p increases linearly with temperature. It is also notable that the order of C_p of the ILs was consistent across all temperatures within the measured range. The complete heat capacity data is found in the appendix, Table 11. and highlights a correlation between C_p and molecular weight across all measured temperatures. Generally, higher ionic weight leads to a higher

C_p . It was found that ILs with bulky quaternary cations have a significantly higher C_p than two-dimensional cations such as imidazolium species. For example, [P₆₆₆₁₄][DEHP] had a C_p 4x that of [C₄(C₁Im)₂][NTf₂], making clear the vast variation of C_p exhibited by ILs - which can be attributed to the number of energy storage modes within the ionic structures. For the imidazolium and pyrrolidinium ILs, C_p was greater for species with a greater ionic mass since, in most cases, more atoms in a structure leads to an increase in energy storage modes which results in a higher C_p of the substance. This is especially true when the added weight is the result of extending alkyl substituents, where the bonds have many modes of rotation and vibration. For [C_nmIm][NTf₂] ILs, the addition of a CH₂ group results in an incremental increase of between 30 - 40 J/molK.^{96,110,47,111} The data collected is consistent with previous studies that have shown that an increase in C_p occurs from monocation to dication for these same reasons.¹¹² However, the C_p of [C₁₀(C₁Im)₂][NTf₂]₂ was recorded as only 1.5x that of [C₄(C₁Im)₂][NTf₂], which is much less substantial than the increase in C_p observed with the 3-dimensional, bulky ionic species. Interestingly, despite [m-xyl-(C₈Im)₂][NTf₂]₂ having a greater molecular weight than [N_{888H}][DEHP] (744.52 g/mol and 676.11 g/mol respectively) its C_p was found to be lower (944.8 ± 0.2 and 1361.5 ± 0.3 at 100 °C). The lower C_p is likely caused by the limited degrees of freedom found in the benzene ring of the cation compared with the long alkyl chains on the ammonium. However, it is worth noting that [N_{888H}][DEHP] has a notably high C_p for its mass and this may have more impact than the xylene.

Of the ILs studied, [P₆₆₆₁₄][DEHP] had the highest C_p , followed by [N_{888H}][DEHP] which had a C_p 410.4 ± 1.8 J/mol·°C less at 20 °C and 360.6 ± 0.9 J/mol·°C at 120 °C. It is logical that [P₆₆₆₁₄][DEHP] would have a higher C_p than [N_{888H}][DEHP] because it has more hydrocarbon chains and therefore more energy storage modes. The high C_p of the bulky quaternary ILs in comparison to the linear DILs is due to the extensive degrees of freedom of the long alkyl chains. The weaker charge density of the ionic species likely enables more freedom of movement as well.

Table 3 – A comparison of [C₄(C₁Im)][NTf₂] C_p measurements in this study and in the literature.

Source	C_p /J·mol ⁻¹ ·K ⁻¹ 40 °C	Method of Recording	Drying Stage Included in the Method?
This Paper	459.4 ± 0.2	Modulated DSC	Yes – 45 min at 100 °C inside DSC instrument (pin-hole method)
[113]	575.1	Calvet type calorimeter	Yes – cell filled with sample in inert gas
[114]	565.1 ± 2.3 (25 °C)	Calorimeter	Not specified
[115]	575.6 ± 0.2 575.0 ± 0.2	DSC - isothermal step method with rate of 0.25 °C/min	Dried for 3 days before experiment but not in the instrument
[116]	575.9	DSC - continuous method-standard zone, with a scanning rate of 2 °C/min	Dried prior to testing but not in instrument
[96]	544.0 ± 27.2	DSC - sapphire method	Yes – 1 h at T = 130 °C inside DSC instrument

Upon comparing the $[C_4(C_1Im)][NTf_2]$ C_p data with other studies, large discrepancies were found. Table 3. highlights the values obtained at 40 °C and the methods used to collect these measurements, as well as whether a drying stage was present in the procedures. Few methods in the comparison studies involved a drying stage after loading the sample into the instrument, and those that did reported lower a C_p also (however not as significantly lower as was recorded in this investigation).⁹⁶ The C_p data collected in this study should be precise due to the care taken in insuring samples contained as little moisture as possible. However, if samples were marginally wet, and moisture was lost in situ (after the programmed drying stage, at the end of which the final sample mass was taken) the mass would in fact be lower than the defined mass taken by the machine. This would result in a C_p measurement that was shifted lower than the true value. This would seem to explain the discrepancies, although $[C_4(C_1Im)][NTf_2]$ is not a very hydroscopic species so variations due to water content are expected to be insignificant.

In other IL species, such as quaternary phosphonium-based carboxylate ILs, water saturation has been shown to significantly increase the C_p - variations of up to 78.3% were reported between pure $[P_{66614}][ButO]$ and when saturated with 16.7 wt% H_2O .¹¹⁷ However, this is a very high level of saturation compared to what would occur from small time periods of exposure to the atmosphere, and therefore much less significant variations would occur naturally from water absorption in ambient conditions.

7.4. Viscosity (μ , ν) and Density (ρ) of Neat ILs

As discussed in the introduction, new classes of EV motor lubricants and thermal fluids must exhibit low viscosities to facilitate increasing motor speeds and higher operating temperatures in new generation vehicles. This property enables lubrication and protection of fast-moving parts without contributing resistance to their motion. It also allows the fluid to effectively dissipate heat away from the high temperature area by reducing the resistance to flow. High density is also important for the heat transfer ability of the fluids as this ensures that there is a higher mass of heat carrying media per unit volume, resulting in high per volume heat absorption.²³ Therefore, it is critical to measure these properties in the synthesised ILs and observe how these behaviours are affected by temperature.

Table 4 - Viscosity and density measurements obtained with a viscometer.

IL	Dynamic Viscosity, μ (mPa·s)		Kinematic Viscosity, ν (mm ² /s)		Density, ρ (g/cm ³)	
	T=20°C	T=100°C	T=20°C	T=100°C	T=20°C	T=100°C
[C ₄ (C ₁ Im)][NTf ₂]	63.21 (± 0.19)	6.45 (± 0.01)	43.92 (± 0.12)	4.72 (± 0.01)	1.439	1.367
[C ₁₀ (C ₁ Im) ₂][NTf ₂] ₂	993.41	29.45	678.83	21.10	1.463	1.396
[C ₁₀ (C ₁ Pyrr) ₂][NTf ₂] ₂	2445.10*	48.78	1721.80	35.92	1.420	1.358
[P ₆₆₆₁₄][DEHP]	1863.00	66.68	2048.50	77.50	0.909	0.860
	α 1045 ¹¹⁸	49.5 ¹¹⁸		59.00 ¹¹⁹		

α = measured at 23 °C, * viscosity above the recommended instrument limit.

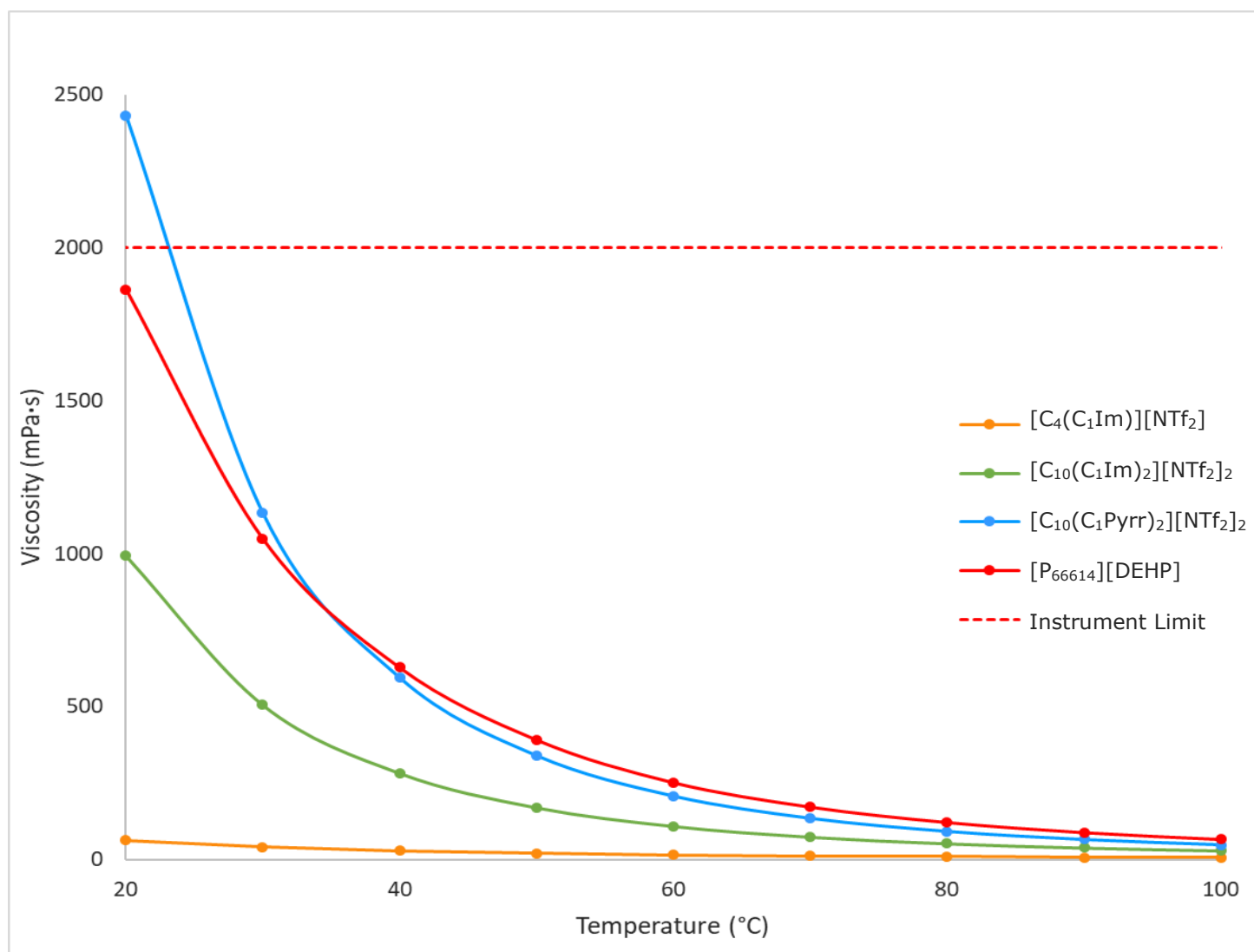


Figure 10 - Experimental viscosity of dried ILs from 20 °C to 100 °C.

It is well documented that anion selection has a significant impact on the viscosity of an IL.⁷² Amongst the common anionic species studied, the $[\text{NTf}_2]^-$ anion has been reported to most drastically decrease the viscosity of a range of IL species.¹²⁰ This is due to a combination of the anion's minimal basicity and moderate weight - the inability of $[\text{NTf}_2]^-$ to form strong H-bonds has a much greater effect than the van der Waals interactions it encourages from its size.¹²¹

Many works have noted an increase in viscosity as a result of increases in the length of alkyl side chains on the cation.^{122,123,124} Many have theorised that this is a result of increased van der Waals interactions from the longer chains.^{121,122} However, computational simulations have led to the theory that as chain length exceeds 4 carbons, (up to C12), imidazolium ILs arrange as microstructured fluids, with both non-polar domains and ionic domains.^{120,125} This likely decreases ion mobility, and therefore the fluid becomes more viscous. Visually, the $[\text{m-xyl}-(\text{C}_8\text{Im})_2][\text{NTf}_2]_2$ ILs appeared to be highly viscous, and this would have been the result of the long octyl chains on the imidazolium rings, combined with π - π stacking of the benzene groups in the functionalised linker.

Figure 10. shows that across the 4 ILs studied, viscosity differences were much more significant at lower temperatures, becoming more similar at higher temperatures. $[\text{C}_4(\text{C}_1\text{Im})][\text{NTf}_2]_2$ measured the smallest range in viscosity (56.7607 mPa·s), with the other ILs having the following ranges: $[\text{C}_{10}(\text{C}_1\text{Im})_2][\text{NTf}_2]_2$ (963.96 mPa·s), $[\text{P}_{66614}][\text{DEHP}]$ (1796.32 mPa·s), $[\text{C}_{10}(\text{C}_1\text{Pyrr})_2][\text{NTf}_2]_2$ (2396.32 mPa·s).

As anticipated from previous studies, $[\text{C}_4(\text{C}_1\text{Im})][\text{NTf}_2]_2$ was significantly less viscous than the dicationic IL species. The small size of the cation enables free movement and an ordered arrangement with reduced internal friction compared to the bulkier dicationic ILs. This is supported by the fact that despite lower viscosities were displayed, density was recorded as being in a similar range to the dicationic species (between $[\text{C}_{10}(\text{C}_1\text{Im})_2][\text{NTf}_2]_2$ and $[\text{C}_{10}(\text{C}_1\text{Pyrr})_2][\text{NTf}_2]_2$).

As seen in Table 3. the dicationic pyrrolidinium IL is much more viscous than the dicationic imidazolium species, despite having a similar structure (10 carbon alkyl chain linker and methyl side chains). At temperatures of up to 70 °C, the pyrrolidinium viscosity was recorded as more than two times greater than that of the imidazolium species (for example: 598.77 and 282.96 mPa·s respectively at 40 °C). This difference is likely a result of the more localised charges in the pyrrolidinium species leading to stronger electrostatic interactions between the ions and therefore there being less ability for ions to show free movement and fluidity. In contrast, the positive charge on the nitrogen atoms in the imidazolium cations are delocalised through resonance stabilisation from the aromatic ring, and therefore the charge density is lowered. This leads to weaker electrostatic attraction between charged species and therefore more ability for free movement and fluidity.

On the other hand, $[\text{C}_{10}(\text{C}_1\text{Pyrr})_2][\text{NTf}_2]_2$ displayed the lowest density values out of the imidazolium and pyrrolidinium ILs measured. This suggests that the composition of the liquid lacks order and instead, a loose arrangement of cations and anions with potential entanglement and holes is more likely. This may also justify the IL's resistance to flow, if the long carbon chains are tangled at various angles, rather than arranged in parallel, where cations can slide over one another. It is a common trend for $[\text{NTf}_2]^-$ ILs with high viscosities to display low densities, and investigations into the phenomenon align with the justifications relating to entanglement and lack of order that are made in this work.¹²⁴

$[\text{P}_{66614}][\text{DEHP}]$ was the only IL where higher kinematic viscosity than dynamic viscosity was recorded. This is most likely due to its relatively high dynamic viscosity but very low density ($< 1 \text{ g/cm}^3$). Since kinematic viscosity is calculated by dividing the dynamic viscosity by density, a larger value is obtained.

This shows that when force is applied, the IL flows faster than the other species, although a reasonable force is needed to get the fluid to flow at a constant rate. This behaviour is a result of the long alkyl substituents on the cation which make it incredibly bulky and asymmetric, leading to a slightly more exaggerated scenario of that observed for $[C_{10}(C_1\text{Pyrr})_2][\text{NTf}_2]_2$. Interestingly, from 40 °C $[P_{66614}][\text{DEHP}]$ displayed the highest viscosity values, showing that the kinetic energy obtained at higher temperatures was less efficiently converted into movement of the molecules compared to the other ILs. This shows the extent of the entanglement of alkyl chains between both the cations and anions.

Density measurements of the ILs clearly shows that density decreases linearly with increasing temperature. This experiment placed the imidazolium and pyrrolidinium ILs at densities in the range of 1.44 – 1.36 g/cm³, whereas $[P_{66614}][\text{DEHP}]$ displayed a much lower density range of 0.91-0.86 g/cm³.

7.5. ILs as EV fluid additives

To test IL capabilities as potential wet e-motor fluid additives, studies were carried out using poly- α -olefin (PAO) non-polar base oils provided by Lubrizol[®]. Three PAO oils with varying viscosity were used: PAO6 (6 mm²/s), PAO4 (4 mm²/s), and PAO2 (2 mm²/s) - with the quoted kinematic viscosity being the value at 100 °C. These base oils provide a good representation of the lubricants and thermal fluids used in EVs before additive species are introduced.

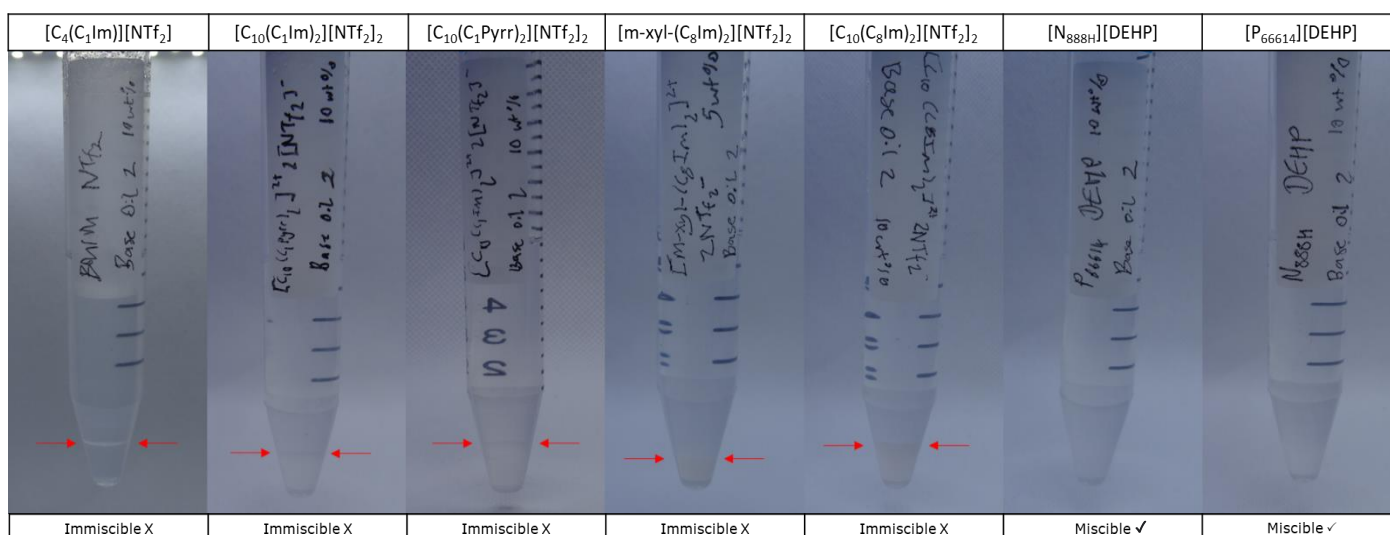


Figure 11 - Miscibility tests of the IL species with PAO4 at a 10 wt% concentration of IL.

7.5.1. Miscibility

Miscibility tests were conducted with 0.5 g IL in 4.5 g PAO4 – i.e. 10 wt% mixtures. The exception to this was $[m\text{-xyl-(C}_8\text{Im)}_2][\text{NTf}_2]_2$, where a 5 wt% mixture was made due to having a small quantity of the pure product (a result of achieving a low yield in the synthesis). The mixtures were shaken vigorously by hand for 30 seconds before being mixed further on a Heidolph[®] Multi Reax vortexer for 20 min at 2000 RPM.

As seen in Figure 11. $[N_{888H}][\text{DEHP}]$ and $[P_{66614}][\text{DEHP}]$ were the only ILs miscible in the PAO base oil – in line with previously published findings.¹²⁶ The other IL additives formed cloudy emulsions upon vigorous shaking, which immediately began separating into two phases with the IL falling to the

bottom of the vessel. The phase boundaries (indicated by the red arrows) were easily identifiable due to the clear differences in densities and refractive indexes.

The miscibility of the contaminated $[C_{10}(C_8Im)_2][NTf_2]_2$ was tested to give insight into potential solubility of the pure IL due to containing long alkyl chains on either side of the structure. However, the impure IL was still immiscible. It is likely that due to its relatively small two-dimensional structure and lack of alkyl chains. It has been suggested that two-dimensional imidazolium cations cannot effectively dissolve in oils, whereas three-dimensional quaternary ions with large hydrocarbon chains have excellent miscibility in non-polar hydrocarbon oils.¹²⁶ The proposed reasoning for this is that the low charge density of the ions, due to the long alkyl chains, reduce interionic interactions, and in turn reduce the effective polarity of the IL, making the species more oil-like.

It has been proposed that for an IL to be oil-soluble, both the cation and anion must be oil soluble.¹²⁷ It has been proposed that for miscibility in such environments, the anion must also contain at least one alkyl chain with four or more carbons.⁷⁷ Therefore, small inorganic anions, such as $[BF_4]^-$, $[PF_6]^-$, or $[Tf_2N]^-$ prevent ILs from being oil-soluble as these anions cannot be dissolved in nonpolar oils.¹²⁷

There is very limited research that investigates improving the solubility of oil immiscible ILs in non-polar base oils with additives such as dispersants, detergents or cosurfactants. However, in theory this could be possible as such additives could bind to the polar ILs and evenly disperse the ions throughout the fluids. An example of this being successful is seen in a 2008 study where 1% of a common detergent and dispersant were used to disperse imidazolium $[BF_4]^-$ and $[PF_6]^-$ species in Group III XHVI grade base oil and resulted in significant anti-wear properties.¹²⁸ This will be an important area of future research if small quantities of high performance ILs can be used as additives in multigrade base oils to improve boundary lubrication or bulk thermophysical properties of the oils. It is a more economically effective solution than using neat ILs and allows a range of performance enhancing additives to be used simultaneously.

As a result of the miscibility tests, $[N_{888H}][DEHP]$ and $[P_{66614}][DEHP]$ were used to make blends with all three PAO base oils at 1, 2, 5 and 10 wt% concentrations. ILs were dried at 50 °C under $<10^{-1}$ pressure for 24 h before making the mixtures to remove water and therefore improve the accuracy of the concentrations, as well as reducing the interference of this impurity in later obtained measurements. Despite this, significant time was taken to precisely measure the mass of the viscous liquids and time restraints meant that drying couldn't be carried out between making every mixture. For this reason, it can be assumed that the ILs would've become marginally water-saturated during the preparations – although the impact of water likely would have been negligible. As expected, the ILs were fully miscible at all concentrations and did not display separation after multiple months in ambient conditions, showing excellent stability.

It is important to note that most of these mixtures do not comply with the International Lubricants Standardization and Approval Committee (ILSAC) GF-5/6 specifications that phosphorus concentrations do not exceed 800 ppm.¹²⁹ For the IL species to meet this requirement, $[N_{888H}][DEHP]$ concentration in the base oil blends can be a maximum of 1.74 wt% and $[P_{66614}][DEHP]$ 1.04 wt%.⁸⁰ The reason for this limit is that phosphorus causes poisoning of catalytic converters and phosphate formation on catalyst surfaces leads to pore blocking which further decreases activity.¹³⁰ Despite this, studying mixtures at higher concentrations provides better insight into the effects of IL additives in hydrocarbon oils. Moreover, this should not be considered an issue when designing lubricants or additives for fully electric vehicles which don't require a catalytic converter, since combustion engines are not present. It also should not be considered an issue for transmission fluids which are contained in a sealed housing, isolated from causing any catalytic damage. However, it means that these fluids would not be suitable for use in engine bearings in HEVs.

7.5.2. Viscosity (μ , ν) and Density (ρ)

It was important to determine the impact of the IL additives on the bulk viscosity and density properties of the base oil mixtures. The neat PAO oils already exhibit desirable viscosity and density properties which should aim to be maintained with addition of the ILs, which provide improved anti-wear and friction reduction properties to the base oils. Therefore, the dynamic viscosity, kinematic viscosity and density of the neat base oils and their IL blends were recorded from 20 °C to 100 °C to make detailed comparisons with.

As with previous viscosity and density tests in this study, ideal results would exhibit a fluid with low viscosity over a broad temperature range to ensure the lubricant reduces friction significantly in fast moving mechanical parts – such as the high RPM E-motor. A high viscosity would inhibit the motor from reaching high speeds and therefore hinder performance. A high density is ideal for the heat transfer properties of the fluid, ensuring they have a high carrier mass per unit volume, enabling greater absorption of heat per volume of fluid. This is most important at high temperatures where thermal transfer away from mechanical sources of heat is crucial to preventing mechanical issues and thermal degradation of chemical components of the system such as greases and lubricants and various additives.

Table 5 - Viscosity and density of IL-base oil mixtures.

PAO no.	[P ₆₆₆₁₄][DEHP] Additive (wt%)	Dynamic Viscosity, μ (mPa·s)		Kinematic Viscosity, ν (mm ² /s)		Density, ρ (g/cm ³)	
		T=20°C	T=100°C	T=20°C	T=100°C	T=20°C	T=100°C
-	100%	1863	66.68	2048.5	77.50	0.909	0.860
		^a 1045 ¹¹⁸	^a 49.5 ¹¹⁸			^a 0.91 ⁵⁹	
6	-	59.80	4.66	72.66	6.02	0.823	0.774
6	1%	59.83	5.81	72.63	5.81	0.824	0.775
6	2%	60.68	4.53	73.61	5.84	0.824	0.775
6	5%	63.26	4.66	76.52	5.99	0.827	0.778
6	10%	78.48	5.25	94.49	6.72	0.831	0.782
4	-	31.94	3.06	39.16	3.99	0.816	0.766
4	1%	32.06	3.08	39.24	4.01	0.817	0.767
4	2%	32.70	3.10	40.02	4.04	0.817	0.767
4	5%	33.60	3.17	41.02	4.12	0.819	0.770
4	10%	40.90	3.68	49.63	4.75	0.824	0.775
2	-	7.09	1.24	8.93	1.67	0.793	0.741
2	1%	7.37	1.29	9.27	1.73	0.795	0.742
2	2%	7.55	1.31	9.48	1.76	0.796	0.743
2	5%	7.88	1.36	9.87	1.82	0.798	0.746
2	10%	11.16	1.58	13.89	2.11	0.804	0.751

Viscosity and density measurements of the PAO-IL blends were only recorded for the $[P_{66614}][DEHP]$ mixtures as the instrument was not compatible with $[N_{888H}][DEHP]$, being an acidic species. However, $[N_{888H}][DEHP]$ was found to have a $\nu = 178 \text{ mm}^2/\text{s}$ at $23 \text{ }^\circ\text{C}$ and $\nu = 13.6$ at $40 \text{ }^\circ\text{C}$. The μ , ν , and ρ of $[P_{66614}][DEHP]$, the neat PAO base oils and various %wt $[P_{66614}][DEHP]$ PAO blends at $20 \text{ }^\circ\text{C}$ and $100 \text{ }^\circ\text{C}$ can be seen in Table 5. Much like the viscosity and density data recorded for the pure ILs, the base oil mixtures and neat oils showed decreases in viscosity and density with increasing temperature.

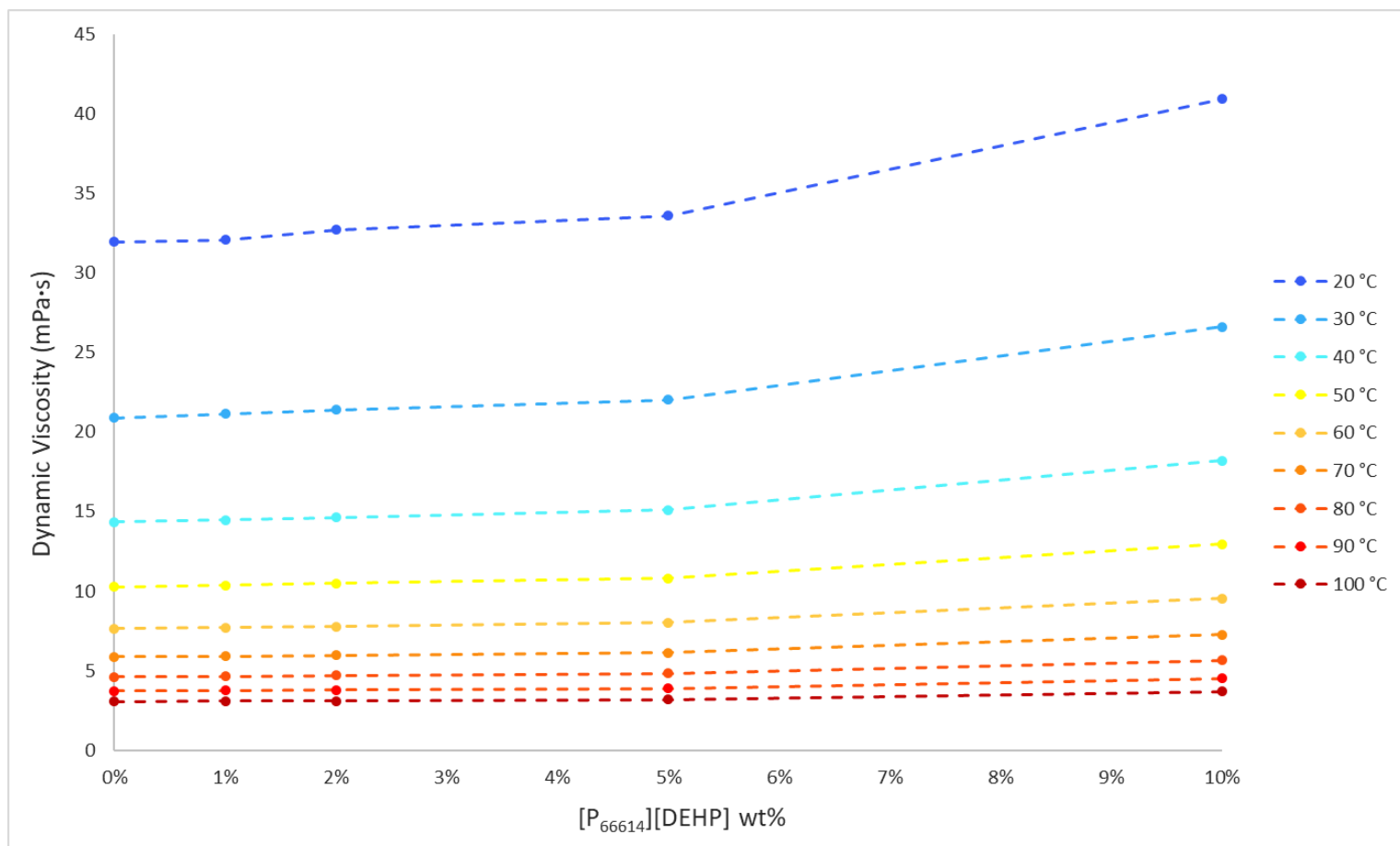


Figure 12 - Dynamic viscosity in relation to the concentration of $[P_{66614}][DEHP]$ in PAO4.

It was calculated that the viscosity of PAO 4 was on average 97% less than $[P_{66614}][DEHP]$. The significantly greater viscosity of the IL meant that when used as an additive, $[P_{66614}][DEHP]$ lead to an increase in viscosity of the mixture compared to the neat base oil. However, somewhat surprisingly, the relationship between the viscosity and $[P_{66614}][DEHP]$ additive %wt concentration was not found to be linear. Figure 12. displays this relationship visually and shows that the influence of the concentration on viscosity is much less prominent at lower concentrations, where the plots are near horizontal up until 5%, where the gradient becomes much steeper to reach the next data point at 10 wt%. For 1, 2 and 5 wt% mixtures with PAO4, an average viscosity increase of $0.15 \text{ mPa}\cdot\text{s}$ (± 0.002) occurred per added 1% IL. However, the 10 wt% mixture showed an increase of $0.39 \text{ mPa}\cdot\text{s}$ per 1% added. This behaviour is advantageous as it has been found that small concentrations of IL additives can have a significant effect on the anti-wear properties of the bulk fluid. Therefore, the positive

effects of the IL can be taken advantage of without the negative impact of drastically increased viscosity.

PAO6, the most viscous of the PAO oils, showed the largest increases in kinematic viscosity with the IL additives. 10 wt% [P₆₆₆₁₄][DEHP] in PAO6 resulted in a 30% increase in kinematic viscosity of the oil at 20 °C. However, interestingly lower wt% mixtures lead to a small decrease in viscosity in many cases. The largest decrease was calculated as 5.67% for the 2 wt% [P₆₆₆₁₄][DEHP] PAO6 mixture at 90 °C. These unusual changes occurred at higher temperatures (≥60 °C) and at low viscosities; therefore, it is possible that the trend is superficial and merely caused by instrument error or low sensitivity. However, if this is true, the error is much larger than the ±0.1% reported by the manufacturer.

Figure 13. shows the positive linear relationship between density and [P₆₆₆₁₄][DEHP] concentration – as more IL additive was used the density increased. This trend was also found to be present for mixtures with PAO6 and PAO2, and these graphs can be found in the appendix, Figure 18. Interestingly, slight variations from the trendline occurred with the 1 wt% mixtures with all three base oils – in the case of 1 wt% [P₆₆₆₁₄][DEHP] in PAO4 at 20 °C, 60 °C, 70 °C and 80 °C, the density was surprisingly higher at 1 wt% than at 2 wt%. However, changes in density were marginal and could be a result of instrument error or external factors such as moisture content. The largest increase in density was given by 10 wt% IL in PAO2 at 70 °C with an increase of 0.011 g/cm³ – this is only a 1.4% increase from the neat base oil, showing just how marginal the changes in density were.

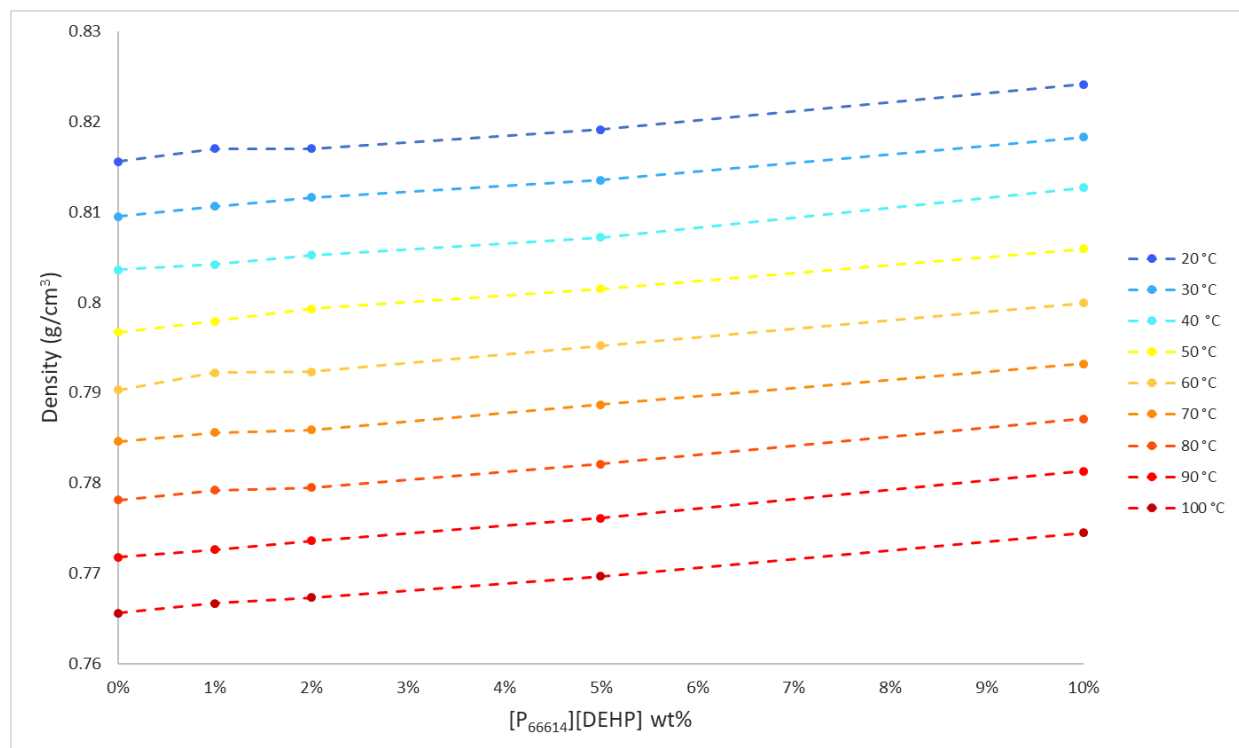


Figure 13 - Density in relation to concentration of [P₆₆₆₁₄][DEHP] in PAO4.

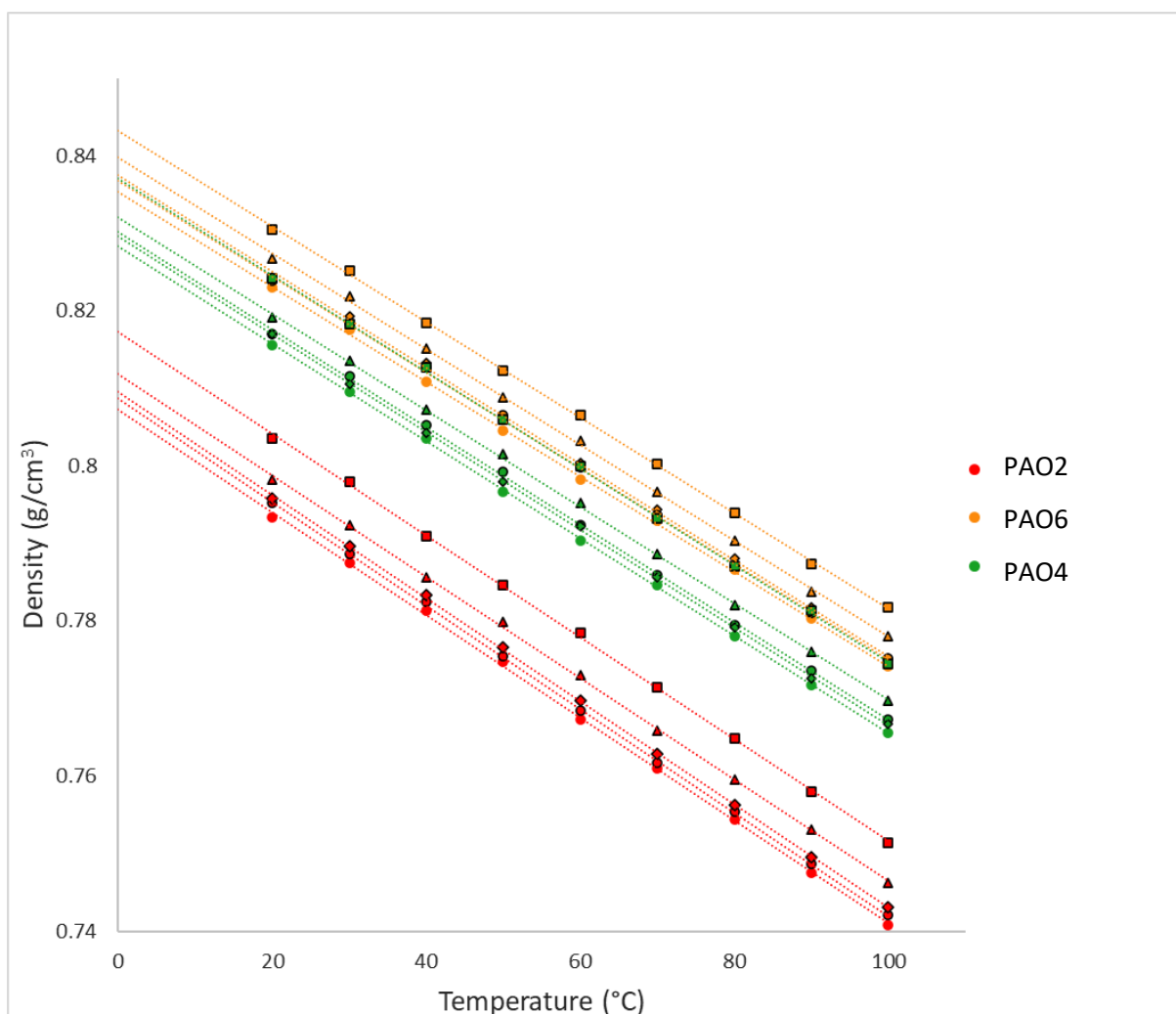


Figure 14 - Density of IL-base oil mixtures. Where \square = 10 wt%, \triangle = 5 wt%, \diamond = 2 wt%, \circ = 1 wt%.

It can be seen in Figure 14. that the relationship between density and temperature was linear and that the rate of change was uniform across all studied fluids (shown by the parallel trendlines). The graphical data has been extrapolated to predict the densities from 0 °C to 20 °C. The highest predicted density was found to be 0.843 g/cm³ for 10 wt% [P₆₆₆₁₄][DEHP] in PAO6. The graph also makes visually clear that the PAO6 and PAO4 mixtures had densities much more similar than PAO2 blends despite the differences between the base oils being equivalent. An overlap occurred between the base oil blends where it was recorded that 10 wt% IL in PAO4 had a higher density than the neat PAO6 and its 1 wt% IL blend.

7.5.3. Viscosity Index, VI

In 1929, Dean and Davis developed the Viscosity Index, VI, – an entirely empirical parameter which ranks the kinematic viscosity of oils based on their stability to increases in temperature.¹³¹ VI is widely adopted in the automotive industry to compare engine oils and ensure that efficient lubrication is achieved across the entire operating temperature range. The value allows the industry to immediately determine if a lubricant is functional at both high and low temperatures, given by a high VI. Most refined mineral oils have a viscosity index value of approximately 100, indicating a good relationship between viscosity and temperature, whereas modern synthetic oils have improved values closer to 150.¹³² In typical motor oils, a higher VI indicates that there are not significant losses in viscosity at higher temperatures, which can result in losses of boundary lubrication and increased wear to mechanical parts.¹³³ This makes higher VI lubricants generally more desirable within the lubricant industry as ideal lubricants maintain a relatively constant viscosity despite temperature changes.¹³⁴

Table 6 - Viscosity index of the IL-base oil mixtures.

PAO No.	IL Additive	Kinematic Viscosity (mm ² /s)		Viscosity Index
		T=40°C	T=100°C	
-	[N888H][DEHP]	178 ⁹⁴	13.6 ⁹⁴	60
-	[P66614][DEHP]	700.28	77.504	193
		528.05 ¹¹⁹	59.00 ¹¹⁹	181 ¹¹⁹
		429 ⁷⁷	49.5 ⁷⁷	177 ⁷⁷
6	-	24.526	6.0168	150
6	1 wt% [P66614][DEHP]	30.414	5.8080	137
6	2 wt% [P66614][DEHP]	30.768	5.8379	136
6	5 wt% [P66614][DEHP]	31.859	5.9941	136
6	10 wt% [P66614][DEHP]	38.482	6.7221	132
4	-	17.825	3.9939	123
4	1 wt% [P66614][DEHP]	17.999	4.0132	122
4	2 wt% [P66614][DEHP]	18.174	4.0364	122
4	5 wt% [P66614][DEHP]	18.681	4.1207	123
4	10 wt% [P66614][DEHP]	22.371	4.7460	135
2	-	5.1335	1.6735	-
2	1 wt% [P66614][DEHP]	5.2383	1.7343	-
2	2 wt% [P66614][DEHP]	5.3382	1.7586	-
2	5 wt% [P66614][DEHP]	5.5477	1.8159	-
2	10 wt% [P66614][DEHP]	7.3566	2.1057	75

VI measurements were obtained using viscosity index calculators from kinematic viscosity values at 40 °C and 100 °C. As shown in Table 5., [P₆₆₆₁₄][DEHP] has very effective viscosity/temperature stability with a VI of 193. In effect, base oil mixtures with this IL resulted in mixtures with high VIs also. Although, interestingly the IL-base oil blends in most cases resulted in lower VI values than the neat base oils. For PAO6 additive blends, the VI was very consistent despite changing [P₆₆₆₁₄][DEHP] concentration (2 and 5 wt% IL both gave a VI value of 136). It was also found that increasing [P₆₆₆₁₄][DEHP] concentration in PAO6 resulted in a trend of overall decreasing VI (a drop of 6 VI units was observed from 1 wt% [P₆₆₆₁₄][DEHP] to 10 wt%). This however was not the case for PAO4 which saw VI increase from 123 to 135 from 0 wt% IL to 10 wt%. It is also noteworthy that the VI of PAO4 wasn't found to change at all for 0, 1, 2 and 5 wt% IL additive blends. This mirrors the previous viscosity interpretations above, stating that the bulk viscosity wasn't influenced as strongly by the IL up until 10 wt% [P₆₆₆₁₄][DEHP] concentration. PAO2 VI data couldn't be calculated due to the fact that a minimum kinematic viscosity of 2 mm²/s is required for the calculations and, apart from the 10 wt% IL blend, all viscosity values at 100 °C were below this.

VI is a widely adopted tool which highlights some interesting properties; however, it is important to consider the inherent limitations of the technique:

- Due to the nature of the calculations, very small viscosity differences below about 5.5 mm²/s can lead to very large VI differences, making the rankings of low viscosity substances misleading.¹³⁵
- It can be argued that comparing viscosity at 40 °C and 100 °C isn't an ideal indication of the substance's behaviour over the full operating temperature range of its potential application.

In support of the second point, it is noteworthy that between 20 °C and 40 °C the IL and base oil mixtures displayed an average loss of viscosity of 53.2% with the neat [P₆₆₆₁₄][DEHP] IL having the largest loss of 65.8% between these temperatures. Whereas the viscosity/temperature graphs tended to smooth out as temperature was increased, showing less drastic variations in viscosity at higher temperatures. It is logical to assume that at temperatures below 20 °C, the liquids would be drastically more viscous and therefore further investigation would be needed to determine whether these materials would function effectively in low ambient conditions. There is great importance to this functionality as to be suitable as a lubricant or thermal fluid in a vehicle, the fluid must be multigrade and operate just as effectively in winter and summer temperatures. This is enabled by a higher VI, describing a fluid that undergoes very little change in viscosity over a broad temperature range. Therefore, exhibited is high fluidity at low temperatures, reducing friction in the moving parts, and enough viscosity at high temperatures to ensure that the mechanical parts are sufficiently lubricated and protected from wear.

However, it is crucial to note that a major advantage of ILs, and [P₆₆₆₁₄][DEHP] and [N_{888H}][DEHP] in particular, is their ability to form protective tribofilms at boundary surfaces, even when the viscosity of the fluid is extremely low.¹³⁶ Therefore, a viscosity that would be much too low in a conventional motor oil, leading to mechanical wear and damage, can still be protective when only a small percentage of IL is present in the media. This property could facilitate the advanced lubrication needs of the development of increasingly fast rotating electric motor bearings, as less friction is experienced with such low viscosity fluids without compromising on tribological protection. Therefore, with these specialist fluids, VI should be used cautiously as a tool to be able to easily identify good viscosity stability regarding temperature increases (VI > 100), but a low viscosity across a broad temperature range should be considered a more favourable characteristic than a higher VI.

It is also important to note that for thermal fluids, which have the role of transferring/dissipating heat away from high temperature mechanical components, a high VI isn't beneficial. This is because as the temperature of the components (such as the copper coil in an EV motor) increases, it is beneficial for the fluid to become less viscous as to allow the fluid to quickly move away from the heat source and dissipate the thermal energy or transfer it to areas of the EV that require it.

7.5.4. Thermal Stability

It was crucial to study the thermal stabilities of the IL-base oil mixtures as one of the main aims of the investigation was to identify thermally stable fluids that could operate in the highly demanding environments of wet e-motors. I was also curious if the IL additives could provide thermophysical improvements to the PAO oils.

Table 7 - Thermal stability data of [N_{888H}][DEHP] and [P₆₆₆₁₄][DEHP] PAO base oil mixtures.

PAO No.	IL Additive	$T_{D(Onset)}$ (°C)	$T_{D(1\%)}$ (°C)	$T_{D(Onset)} - T_{D(1\%)}$ (°C)
4	-	233.3	173.4	59.9
4	1 wt% [N _{888H}][DEHP]	242.3	184.2	58.1
4	2 wt% [N _{888H}][DEHP]	242.5	179.3	63.2
4	5 wt% [N _{888H}][DEHP]	237.8	176.4	61.5
4	10 wt% [N _{888H}][DEHP]	224.9	159.5	65.4
-	[N _{888H}][DEHP]	225.3	164.4	60.8
4	1 wt% [P ₆₆₆₁₄][DEHP]	225.1	170.8	54.4
4	2 wt% [P ₆₆₆₁₄][DEHP]	231.8	175.3	56.4
4	5 wt% [P ₆₆₆₁₄][DEHP]	227.1	173.9	53.2
4	10 wt% [P ₆₆₆₁₄][DEHP]	236.7	180.8	55.9
-	[P ₆₆₆₁₄][DEHP]	281.4	191.1	90.3
6	-	247.4	188.8	58.6
6	5 wt% [P ₆₆₆₁₄][DEHP]	235.2	186.7	48.5
2	-	151.6	94.8	56.8
2	5 wt% [P ₆₆₆₁₄][DEHP]	172.6	112.7	59.9

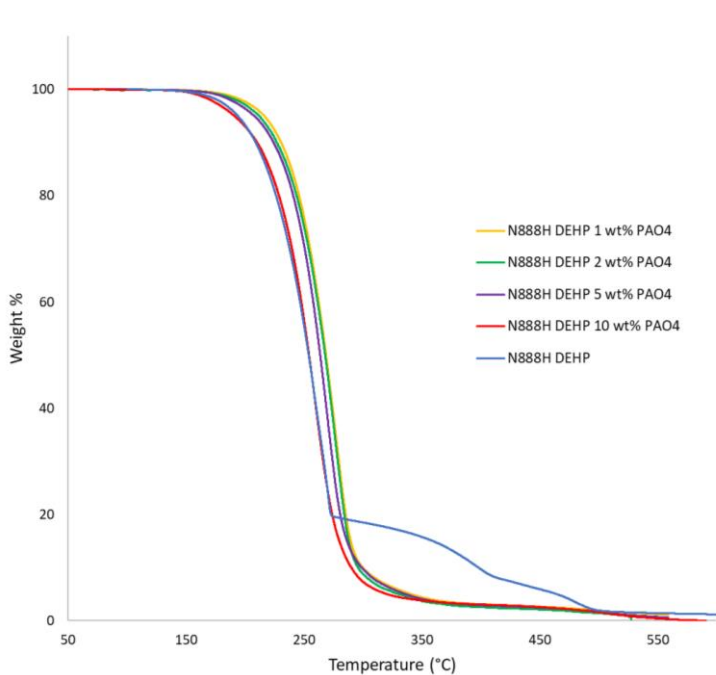


Figure 15- Thermal degradation of $[N_{888H}][DEHP]$ PAO4 blends

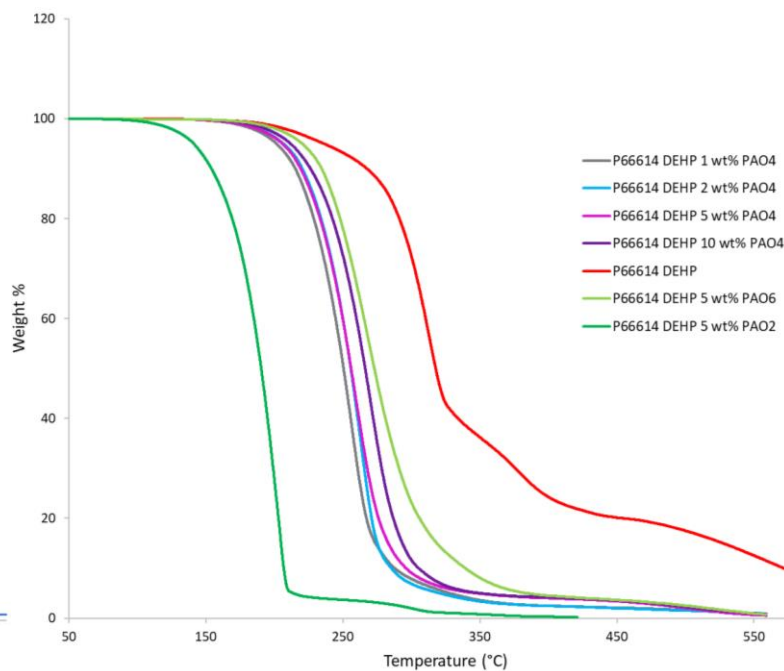


Figure 16 - Thermal degradation of $[P_{66614}][DEHP]$ PAO blends

As seen in Table 7, the addition of $[N_{888H}][DEHP]$ and $[P_{66614}][DEHP]$ to the base oils generally led to increases in their onset temperatures of degradation and 1% mass loss temperatures. The largest increase in $T_{D(1\%)}$ from the neat base oil was with 5 wt% $[P_{66614}][DEHP]$ in PAO2, which gave an improvement in stability of 17.92 °C (an 18 % increase). The addition of 1 wt% $[N_{888H}][DEHP]$ to PAO4 also resulted in a notable improvement in stability of 10.78 °C (a 6.2 % increase from the neat base oil). Interestingly, the mixtures of 1, 2 and 5 wt% $[N_{888H}][DEHP]$ in PAO4 resulted in higher stabilities than those of the neat IL and PAO oil components.

Figure 15, and Figure 16, show the TGA thermograms and make clear that when the IL is used as an additive in the PAO base oils, a much smoother degradation curve is observed. This suggests that the oil media provides stability to the acid-base equilibria and a single-step degradation takes place, as opposed to the multi-step profile of the neat ILs. This single-step thermal degradation behaviour is more similar to the imidazolium and pyrrolidinium ILs studied, as seen in Figure 7.

The neat $[P_{66614}][DEHP]$ IL was found to have the highest stability with a 281.38 °C onset degradation (48.11 °C greater than the PAO4). However, the IL also showed the biggest variation between temperature of onset degradation and 1% mass loss temperature. This may suggest that a slower degradation occurs above its 1% mass loss temperature than was observed for the other samples. Experiments testing the stability of the IL over a longer time period at invariable temperatures would be needed to be carried out to confirm this. Similar experiments have shown that significant decomposition of ILs often occurs at much lower temperatures than T_d onset when these conditions are prolonged for multiple hours – as may occur in the real-life operation of these substances.¹³⁷ In this study, 1% mass loss temperature was recorded with this in mind, giving an average difference of 60.19 °C between T_d onset and 1% mass loss of the data in Table 7. (26.78% lower). However, it is likely that this is still an overestimation of the actual temperature that degradation would occur in a vehicle over longer time frames.

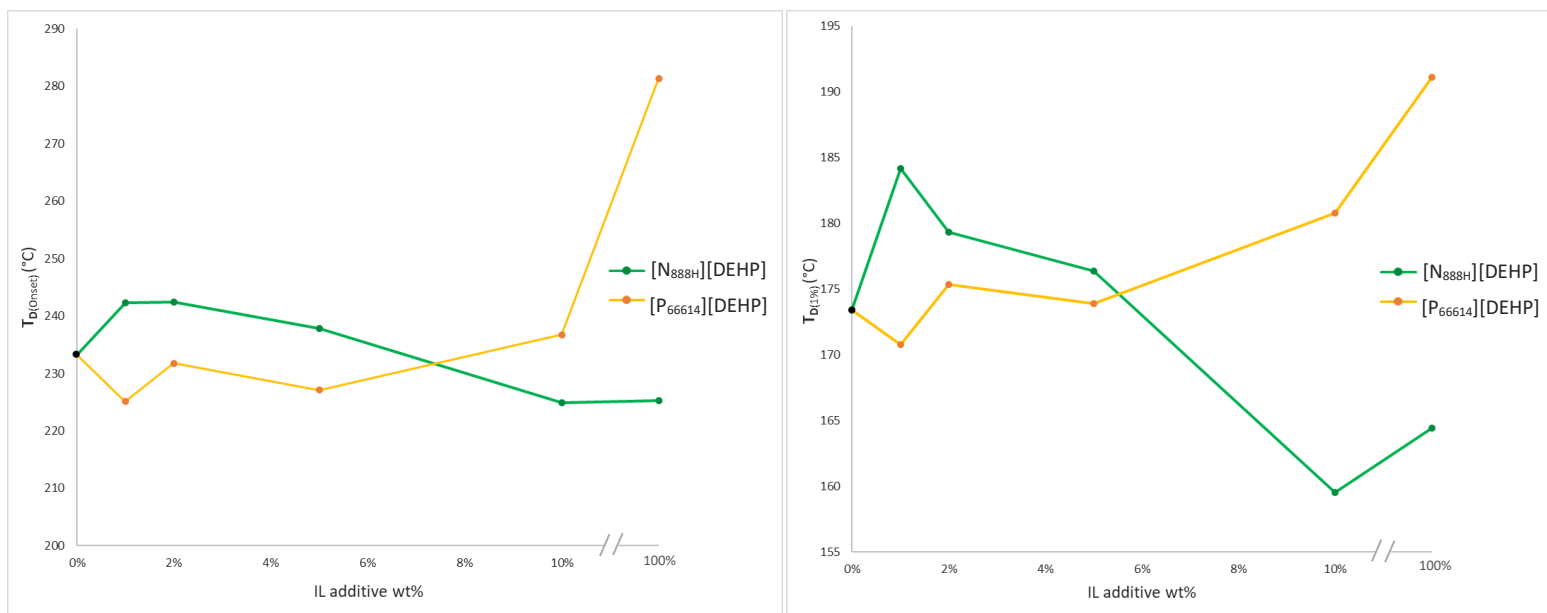


Figure 17 - Thermal stability of [N_{888H}][DEHP] and [P₆₆₆₁₄][DEHP] IL- PAO4 blends in relation to IL additive concentration. (a) stability expressed as temperature of onset degradation, (b) stability expressed as temperature of 1% mass loss of sample.

Figure 17. expresses the data visually and makes clear that very different behaviour was exhibited by the two ILs as PAO additives - likely due to fact that [P₆₆₆₁₄][DEHP] is more thermally stable than PAO4 and [N_{888H}][DEHP] is less. PAO4 shows an increase in $T_{D(1\%)}$ with the addition of 1 wt% [N_{888H}][DEHP], followed by gradual decreases in stability as more IL was added – becoming less stable than the neat PAO base oil between 5 and 10 wt%. In contrast, the base oil shows an initial decrease in $T_{D(1\%)}$ with the addition of 1 wt% [P₆₆₆₁₄][DEHP], followed by an overall trend of increasing stability as more IL was added. Despite this, an anomalous decrease in stability was observed from 2 wt% to 5 wt% [P₆₆₆₁₄][DEHP] in PAO4. When considering onset temperature, the stability of all of the blends are in the ideal range for use in new generation EVs, and appear to be appropriate additive species in cases where neat ILs aren't suitable. However, since the copper windings of electric motors can reach up to 180 °C, only the 1 wt% [N_{888H}][DEHP] PAO4 blend meets the temperature requirements when taking the thermal decomposition temperature as 1% mass loss of the sample.²⁷

The behaviour suggests that other factors may have had more influence on the stability of the blends than just the concentration of the IL in the mixture. For example, factors such as moisture content could have caused variations in the data – however [P₆₆₆₁₄][DEHP] and the PAO oils are hydrophobic substances so it is expected that water absorption from the environment would be minimal. Perhaps a more likely explanation is that the dispersion of ions in the hydrocarbon oils may vary based on the concentration of the IL, forming different structures and clusters which result in different thermal behaviour. Further research would be needed to confirm this.

8. Conclusion

In summary, a range of imidazolium, pyrrolidinium, phosphonium and ammonium ILs were synthesised and their thermophysical properties were measured. From this it can be concluded that the $[\text{NTf}_2]^-$ anion provides superior thermal stability to IL species, as observed by the extremely high T_d of $[\text{C}_{10}(\text{C}_1\text{Im})_2][\text{NTf}_2]_2$ and $[\text{C}_{10}(\text{C}_1\text{Pyr})_2][\text{NTf}_2]_2$ (435.0 °C and 419.6 °C respectively). ILs containing the $[\text{NTf}_2]^-$ anion achieved a T_d that was 143.89 ± 9.51 °C higher than their halide anion equivalents and an average $T_{D(1\%)}$ increase of 116.73 ± 23.98 °C. The anion also had a significant impact on liquid range, inciting fluidity of the ILs at much lower temperatures (such as $[\text{C}_{10}(\text{C}_1\text{Im})_2][\text{NTf}_2]_2$ which appears to be liquid above -61.5 °C). The novel DIL, $[\text{m-xyl}-(\text{C}_8\text{Im})_2][\text{NTf}_2]_2$ also showed an excellent liquid range from -51.6 °C (T_g) to 382.5 °C (T_d), however was visually significantly more viscous than the $[\text{C}_{10}(\text{C}_1\text{Pyr})_2][\text{NTf}_2]_2$, and therefore also unsuitable for use in this application.

As anticipated from the literature, geminal imidazolium and pyrrolidinium DILs proved to exhibit wide liquid ranges which can be attributed to difficulties in packing of the large molecules, preventing the formation of an ordered crystal lattice. However, the DILs exhibited significantly greater viscosities at lower temperatures when compared to the smaller aprotic monocationic IL species. $[\text{C}_{10}(\text{C}_1\text{Im})_2][\text{NTf}_2]_2$ had a kinematic viscosity of 678.83 mm²/s at 20 °C whereas $[\text{C}_4(\text{C}_1\text{Im})][\text{NTf}_2]$ was 43.91 mm²/s (more than 15x smaller). The pyrrolidinium DIL was observed to have an even greater kinematic viscosity of 1721.8 mm²/s at 20 °C. This high resistance to flow limits the thermal management capabilities of the fluids. However, they were all observed to have low viscosities at high temperatures, which is far more important when considering friction reduction and the ability of cooling high temperature mechanical and electrical parts – as this means they will be able to dissipate the heat away from the source quickly. Despite this, the high viscosity of the ILs at lower temperatures could pose an issue for the lubrication of bearings in the motor and transmission as there would be notable resistance from the lubricants. This makes these particular species unsuitable for this application, when used as neat lubricants, as specifically low viscosity lubricants are required to facilitate the high e-motor speeds over a broad temperature range.

Miscibility tests confirmed that even with long aliphatic chains present in imidazolium and pyrrolidinium $[\text{NTf}_2]^-$ DILs, these ILs were insoluble in non-polar PAO base oils, making them inappropriate for use as additives in such base stocks. However, $[\text{P}_{66614}][\text{DEHP}]$ and $[\text{N}_{888\text{H}}][\text{DEHP}]$ showed excellent solubility in a range of PAO base oils. These ILs were found to cause insignificant increases in viscosity of the PAOs, particularly at low wt% concentrations. However, the addition of $[\text{N}_{888\text{H}}][\text{DEHP}]$ and $[\text{P}_{66614}][\text{DEHP}]$ to the base oils generally led to increases in the T_d of the bulk fluid, showing that these IL additives can provide both tribological improvements as well as thermophysical improvements. In addition to this, $[\text{N}_{888\text{H}}][\text{DEHP}]$ was shown to provide the greatest thermal stability improvements at 1 wt% concentrations compared to at higher concentrations, making the additive more economically viable. In contrast, $[\text{P}_{66614}][\text{DEHP}]$ showed an inverse behaviour as a PAO additive, with the IL-base oil blends exhibiting greater stability at higher additive concentrations.

Further investigation is required to determine if these species can overcome the barriers to commercialization in real-life industrial applications, such as economic costs. However, it is promising that the least expensive ILs in this study ($[\text{N}_{888\text{H}}][\text{DEHP}]$ and $[\text{P}_{66614}][\text{DEHP}]$) gave excellent thermophysical properties, particularly at low concentrations as additives in PAO base oils. For this reason, it is likely that ILs could be employed as additive species in lubricants, much like nanoparticles, in the near future to reduce wear and improve the bulk thermophysical properties of fluids. However,

as neat lubricants and heat transfer fluids, the imidazolium and pyrrolidinium [NTf₂]⁻ ILs are currently economically unfeasible for industry use due to such high production costs.

The next stages of research should include determining the compatibility of these fluids with the various materials in the EV machinery, and particularly with the copper coil and other metals present in the mechanical parts. Electrical compatibility is a further field requiring investigation with these liquids, since in this application, the fluids would be in direct contact with electrical currents from the e-motor, as well as areas of potential static build-up. Lastly, the thermal conductivity of the ILs would be a valuable property to investigate as it would provide a better indication of the ability of these species as thermal management fluids.

9. Bibliography

- 1 Department for Transport, Transport and Environment Statistics 2021 Annual Report, <https://www.gov.uk/government/statistics/transport-and-environment-statistics-2021>, (accessed 6 December 2022).
- 2 The Paris Agreement, <https://unfccc.int/process-and-meetings/the-paris-agreement>, (accessed November 2022).
- 3 EEA, *Transport and environment report 2021 Decarbonising: Decarbonising road transport – the role of vehicles, fuels and transport demand*, 2022.
- 4 Department for Transport, Taking charge: the electric vehicle infrastructure strategy, <https://www.gov.uk/government/publications/uk-electric-vehicle-infrastructure-strategy>, (accessed 18 September 2022).
- 5 S. Zheng, X. Zhu, Z. Xiang, L. Xu, L. Zhang and C. H. T. Lee, *Green Energy Intell. Transp.*, 2022, **1**, Article: 100012.
- 6 A. Ibrahim and F. Jiang, *Renew. Sustain. Energy Rev.*, 2021, **144**, 111049.
- 7 E. Rodríguez, N. Rivera, A. Fernández-González, T. Pérez, R. González and A. H. Battez, *Tribol. Int.*, 2022, **171**, Article 107544.
- 8 A. Krings and C. Monissen, *Review and Trends in Electric Traction Motors for Battery Electric and Hybrid Vehicles*, Institute of Electrical and Electronics Engineers, 2020.
- 9 L. I. Farfan-cabrera, *Tribology Int.*, 2019, **138**, 473–486.
- 10 Y. Chen, S. Jha, A. Raut, W. Zhang and H. Liang, *Front. Mech. Eng.*, 2020, **6**, 1–19.
- 11 K. Narita and D. Takekawa, *Lubricants Technology Applied to Transmissions in Hybrid Electric Vehicles and Electric Vehicles*, 2019.
- 12 J. M. Andrew, *Tribol. Lubr. Technol.*, 2019, **75**, 38–44.
- 13 M. Yoshizawa, W. Xu and C. A. Angell, *J. Am. Chem. Soc.*, 2003, **125**, 15411–15419.
- 14 R. A. Mantz and P. C. Trulove, *Ionic Liquids in Synthesis*, Wiley-VCH, 1st edn., 2002.
- 15 H. L. Ngo, K. Lecompte, L. Hargens and A. B. Mcewen, *Thermochim. Acta*, 2000, **258**, 97–102.
- 16 F. Endres, S. Zein and E. Abedin, *Phys. Chem. Chem. Phys.*, 2006, **8**, 2101–2116.
- 17 Z. Chen, S. Liu, Z. Li, Q. Zhang and Y. Deng, *New J. Chem.*, 2011, **35**, 1596–1606.
- 18 J. F. Vélez, M. B. Vázquez-Santos, J. M. Amarilla, B. Herradón, E. Mann, C. del Río and E. Morales, *J. Power Sources*, 2019, **439**, Article 227098.
- 19 Q. Chen, K. Wu and C. He, *Ind. Eng. Chem. Res.*, 2014, **53**, 7224–7232.
- 20 K. Holmberg and A. Erdemir, *Tribology Int.*, 2019, **135**, 389–396.
- 21 K. Holmberg, P. Andersson and A. Erdemir, *Tribol. Int.*, 2012, **47**, 221–234.
- 22 S. F. Tie and C. W. Tan, *Renew. Sustain. Energy Rev.*, 2013, **20**, 82–102.
- 23 M. Beyer, G. Brown, M. Gahagan, T. Higuchi, G. Hunt, M. Huston, D. Jayne, C. Mcfadden, T. Newcomb, S. Patterson, C. Prengaman and M. Shamszad, *Tribol. Online*, 2019, **14**, 428–437.
- 24 O. Access, , DOI:10.1088/1742-6596/364/1/012041.

- 25 R. Shah, B. Gashi, S. González-Poggini, M. Colet-Lagrille and A. Rosenkranz, *Adv. Mech. Eng.*, 2021, **13**, 1–10.
- 26 B. Bilgin and A. Emadi, *IEEE Power Electron. Mag.*, 2014, **1**, 10–17.
- 27 K. Lee, H. Cha and Y. Kim, *App. Therm. Eng.*, 2016, **95**, 348–356.
- 28 X. Wang, B. Li, D. Gerada, K. Huang, I. Stone, S. Worrall and Y. Yan, *Appl. Therm. Eng.*, 2022, **201**, Article: 117758.
- 29 T. Ha, N. G. Han, M. S. Kim, K. H. Rho and D. K. Kim, *Energies*, , DOI:10.3390/en14040956.
- 30 Z. Huang, S. Nategh, V. Lassila, M. Alaküla and J. Yuan, in *IEEE International Electric Vehicle Conference, Greenville, SC, USA*, 2012, pp. 1–8.
- 31 P. Lindh, I. Petrov, J. Pyrhönen, E. Scherman, M. Niemelä and P. Immonen, *IEEE Trans. Ind. Appl.*, 2019, **55**, 4183–4191.
- 32 N. Rivera, J. L. Viesca, A. Garc, J. I. Prado, L. Lugo and A. H. Battez, *Appl. Sci.*, 2022, **12**, Article 8911.
- 33 H. V. Nutt, E. W. Landen and J. A. Edgar, *SAE Trans.*, 1955, **63**, 694–703.
- 34 W. A. A. Mustafa, F. Dassenoy, M. Sarno and A. Senatore, *Lubr. Sci.*, 2021, **34**, 1–29.
- 35 T. Sada, *Tribol. Online*, 2017, **12**, 94–98.
- 36 In *API Base Oil Interchangability Guidelines For Passenger Car Motor Oils And Diesel Engine Oils*, American Petroleum Institute, 2019, pp. 1–33.
- 37 A. S. Sarpal, M. I. S. Sastry, V. Bansal, I. Singh, S. K. Mazumdar and B. Basu, *Lubr. Sci.*, 2012, **24**, 199–215.
- 38 V. Bansal and A. K. Mehta, *Lubr. Sci.*, 2004, **16**, 361–375.
- 39 R. Benda, J. Bullen and A. Plomer, *J. Synth. Lubr.*, 1996, **13**, 41–57.
- 40 T. Welton, *Chem. Rev.*, 1999, **99**, 2071–2083.
- 41 J. S. Wilkes, *Green Chem.*, 2002, **4**, 73–80.
- 42 D. V. Chernyshov and W. C. Shin, *J. Electrochem. Sci. Technol.*, 2014, **5**, 95–104.
- 43 T. Sato, G. Masuda and K. Takagi, *Electrochim. Acta*, 2004, **49**, 3603–3611.
- 44 C. Ye, W. Liu, Y. Chen and L. Yu, *Chem. Commun.*, 2001, **21**, 2244–2245.
- 45 J. F. Brennecke and E. J. Maginn, *AIChE J.*, 2001, **47**, 2384–2389.
- 46 B. Wu, R. G. Reddy and R. D. Rogers, in *Solar Engineering: International Solar Energy Conference (Solar Energy — The Power to Choose)*, ASME, 2001, pp. 445–451.
- 47 J. D. Holbrey, W. M. Reichert, R. G. Reddy and R. D. Rogers, *ACS Symp. Ser.*, 2003, **856**, 121–133.
- 48 P. Wang, S. Liu, L. Lu, X. Ma, Y. He and Y. Deng, *RSC Adv.*, 2015, **5**, 62110–62115.
- 49 C. Araya-López, P. Carrera, A. Torres, L. Pino-soto, E. Quijada-Maldonado, G. Merlet, C. Araya-I, J. Romero, A. Plaza and R. Cabezas, *Thermochim. Acta*, 2022, **714**, Article 179262.
- 50 A. J. Carmichael and K. R. Seddon, *J. Phys. Org. Chem.*, 2000, **13**, 591–595.
- 51 U. Maurya, V. Vasu and D. Kashinath, *Mater. Today Proc.*, 2022, **59**, 1651–1658.

- 52 U. A. Rana, R. Vijayaraghavan, M. Walther, J. Sun, A. A. J. Torriero and D. R. Macfarlane, 2011, 11612–11614.
- 53 P. Walden, *Bull. Acad. Imper. Sci. (St. Petersburg)*, 1914, 405–422.
- 54 P. T. Anastas and J. C. Warner, *Green Chemistry: Theory and Practice*, Oxford University Press, New York, 1998.
- 55 T. L. Greaves and C. J. Drummond, *Chem. Rev.*, 2015, **115**, 11379–11448.
- 56 W. Xu and C. A. Angell, *J. Sci.*, 2003, **302**, 422–425.
- 57 T. Espinosa, J. Sanes, A. E. Jiménez and M. D. Bermúdez, *Wear*, 2013, **303**, 495–509.
- 58 Y. Shi and R. Larsson, *Tribol. Lett.*, 2016, **63**, 1–7.
- 59 Y. Zhou, T. W. Graham, H. Luo, D. N. Leonard and J. Qu, *Langmuir*, 2014, **30**, 13301–13311.
- 60 J. Qu, J. J. Truhan, S. Dai, H. Luo and P. J. Blau, *Tribol. Lett.*, 2008, **22**, 207–214.
- 61 M. D. A. F. J. Carrión and V. J. Sanes, *Tribol. Lett.*, 2019, **67**, 1–10.
- 62 J. L. Anderson, R. Ding, A. Ellern and D. W. Armstrong, *J. Am. Chem. Soc.*, 2005, **127**, 593–604.
- 63 C. M. Jin, C. Ye, B. S. Phillips, J. S. Zabinski, X. Liu, W. Liu and J. M. Shreeve, *J. Mater. Chem.*, 2006, **16**, 1529–1535.
- 64 B. L. Kuhn, B. F. Osmari, T. M. Heinen, H. G. Bonacorso, N. Zanatta, S. O. Nielsen, D. T. S. Ranathunga, M. A. Villetti and C. P. Frizzo, *J. Mol. Liq.*, 2020, **308**, Article 112983.
- 65 R. Wang, H. Gao, C. Ye and J. M. Shreeve, *Chem. Mater.*, 2007, **19**, 144–152.
- 66 Z. K. Reeder, A. M. Adler and K. M. Miller, *Tetrahedron Lett.*, 2016, **57**, 206–209.
- 67 R. Wang, C. Jin, B. Twamley and J. M. Shreeve, *Inorg. Chem.*, 2006, **45**, 6396–6403.
- 68 J. Chang, W. Ho, I. Sun, Y. Tung, M. Tsui and T. Wu, *Tetrahedron*, 2010, **66**, 6150–6155.
- 69 M. M. Obadia, A. Jourdain, A. Sergej, T. Ikeda and E. Drockenmulle, *Polym. Chem.*, 2017, **8**, 910–917.
- 70 J. Wu, L. Mu, X. Feng, X. Lu, R. Larsson and Y. Shi, *Adv. Mater. Interfaces*, 2019, **6**, Article 1801796.
- 71 M. R. O. Vega, J. Ercolani, S. Mattedi, C. A. Ferreira, A. S. Rocha and C. F. Malfatti, *Ind. Eng. Chem. Res.*, 2018, **57**, 12386–12396.
- 72 C. P. Fredlake, J. M. Crosthwaite, D. G. Hert, S. N. V. K. Aki and J. F. Brennecke, *J. Chem. Eng. Data*, 2004, **49**, 954–964.
- 73 I. Minami, M. Kita, T. Kubo, H. Nanao and S. Mori, *Tribol. Lett.*, 2008, **30**, 215–223.
- 74 M. G. Freire, C. M. S. S. Neves, I. M. Marrucho, J. A. P. Coutinho and A. M. Fernandes, *J. Phys. Chem. A*, 2010, **114**, 3744–3749.
- 75 P. A. Z. Suarez, S. Einloft, J. E. L. Dullius, R. F. de Souza and J. Dupont, *Chim. Phys.*, 1998, **95**, 1626–1639.
- 76 J. G. Huddleston, A. E. Visser, W. M. Reichert, H. D. Willauer, G. A. Broker and R. D. Rogers, *Green Chem.*, 2001, **3**, 156–164.
- 77 J. Qu, D. G. Bansal, B. Yu, J. Y. Howe, H. Luo, S. Dai, H. Li, P. J. Blau, B. G. Bunting, G. Mordukhovich and D. J. Smolenski, *Appl. Mater. Interfaces*, 2012, **4**, 997–1002.

- 78 R. González, A. H. Battez, D. Blanco, J. L. Viesca and A. Fernández-González, *Tribol. Int.*, 2010, **40**, 269–277.
- 79 T. Naveed, R. Zahid, R. A. Mufti, M. Waqas and M. T. Hanif, *J. Eng. Tribol.*, 2021, **235**, 1782–1806.
- 80 J. Qu, H. Luo, M. Chi, C. Ma, P. J. Blau, S. Dai and M. B. Viola, *Tribology Int.*, 2014, **71**, 88–97.
- 81 J. Leang, R. Walvekar, T. Nagarajan, Z. Said, M. Khalid and N. M. Mubarak, *J. Mol. Liq.*, 2022, **366**, Article 120274.
- 82 F. Zhou, Y. Liang and W. Liu, *Chem. Soc. Rev.*, 2009, **38**, 2590–2599.
- 83 E. A. Chernikova, L. M. Glukhov, V. G. Krasovskiy, L. M. Kustov, M. G. Vorobyeva and A. A. Koroteev, *Russ. Chem. Rev.*, 2015, **84**, 875–890.
- 84 A. J. Greer, J. Jacquemin and C. Hardacre, *Molecules*, 2020, **5207**, 1–31.
- 85 J. M. P. Franca, C. A. Castro, M. M. Lopes and V. M. B. Nunes, *J. Chem. Eng. Data*, 2009, **54**, 2569–2575.
- 86 R. S. Kalb, E. N. Stepurko, V. N. Emel'yanenko and S. P. Verevkin, *Phys. Chem. Chem. Phys.*, 2016, **18**, 31904–31913.
- 87 R. S. Kalb, M. Damm and S. P. Verevkin, *React. Chem. Eng.*, 2017, **2**, 432–436.
- 88 G. R. Fulmer, A. J. M. Miller, N. H. Sherden, H. E. Gottlieb, A. Nudelman, B. M. Stoltz, J. E. Bercaw and K. I. Goldberg, *Organometallics*, 2010, **29**, 2176–2179.
- 89 L. Liu, B. Wang, H. Yang, W. Chang and J. Li, *Tetrahedron Lett.*, 2011, **52**, 5636–5639.
- 90 C. C. Weber, A. F. Masters and T. M. Maschmeyer, *Angew. Chem. Int. Ed.*, 2012, **51**, 11483–11486.
- 91 I. M. Gindri, D. A. Siddiqui, P. Bhardwaj, L. C. Rodriguez, K. L. Palmer, C. P. Frizzo, M. A. P. Martins and D. C. Rodrigues, *RSC Adv.*, 2014, **4**, 62594–62602.
- 92 K. T. C. Liu, R. S. Haines and J. B. Harper, *Org. Biomol. Chem.*, 2020, **18**, 7388–7395.
- 93 F. D'Anna, P. Vitale, F. Ferrante, S. Marullo and R. Noto, *Chempluschem*, 2013, **78**, 331–342.
- 94 W. C. Barnhill, H. Luo, H. M. Meyer, C. Ma, M. Chi, B. L. Papke and J. Qu, *Tribol. Lett.*, 2016, **63**, 1–11.
- 95 L. Qingshan, M. Lin, Z. Qige, L. Qingshan, M. Lin, Z. Qige and X. Quan, in *Progress and Development in Ionic Liquids*, ed. S. Handy, 2017, pp. 369–412.
- 96 E. Gómez, N. Calvar, Á. Domínguez and E. A. MacEdo, *Ind. Eng. Chem. Res.*, 2013, **52**, 2103–2110.
- 97 S. V. Dzyuba and R. A. Bartsch, *ChemPhysChem*, 2002, **3**, 161–166.
- 98 H. Shirota, T. Mandai, H. Fukazawa and T. Kato, *J. Chem. Eng. Data*, 2011, **56**, 2453–2459.
- 99 D. Blanco, M. Bartolomé, B. Ramajo, J. L. Viesca and R. González, *Thermochim. Acta*, 2017, **648**, 62–74.
- 100 I. Krossing, J. M. Slattery, C. Daguene, P. J. Dyson, A. Oleinikova and H. Weingartner, *J. Am. Chem. Soc.*, 2006, **128**, 13427–13434.
- 101 M. Boumediene, B. Haddad, A. Paolone and M. Draï, *J. Mol. Struct.*, 2019, **1186**, 68–79.

- 102 A. E. Bradley, C. Hardacre, J. D. Holbrey, S. Johnston, S. E. J. Mcmath and M. Nieuwenhuyzen, *Chem. Mater.*, 2002, **14**, 629–635.
- 103 D. B. Cassel, *Mater. Sci.*, 2001, 1–4.
- 104 T. Carnelley, *Philos. Mag. J. Sci.*, 1882, **5**, 180–193.
- 105 J. Shawe, R. Riesen, J. Widmann, M. Schubnell and U. Jörimann, *Mettler Toledo UserCom*, 2000, 1–28.
- 106 M. Kosmulski, J. Gustafsson and J. B. Rosenholm, *Thermochim. Acta*, 2004, **412**, 47–53.
- 107 P. Bonho, A. Dias, N. Papageorgiou, K. Kalyanasundaram and M. Gratzel, *Inorg. Chem.*, 1996, **35**, 1168–1178.
- 108 Z. Zeng, B. S. Phillips, J. C. Xiao and J. M. Shreeve, *Chem. Mater.*, 2008, **20**, 2719–2726.
- 109 C. R. Bender, B. L. Kuhn, C. A. A. Farias, F. I. Ziembowicz, T. S. Beck and C. P. Frizzo, *J. Braz. Chem. Soc.*, 2019, **30**, 2199–2209.
- 110 R. Ge, C. Hardacre, J. Jacquemin, P. Nancarrow and D. W. Rooney, *J. Chem. Eng. Data*, 2008, **53**, 2148–2153.
- 111 Y. U. Paulechka, A. V. Blokhin, G. J. Kabo and A. A. Strechan, *J. Chem. Thermodyn.*, 2007, **39**, 866–877.
- 112 R. Fareghi-alamdari and R. Hatefipour, *Thermochim. Acta*, 2015, **617**, 172–178.
- 113 T. Makino, M. Kanakubo, Y. Masuda and H. Mukaiyama, *J. Solution Chem.*, 2014, **43**, 1601–1613.
- 114 A. V. Blokhin, Y. U. Paulechka, A. A. Strechan and G. J. Kabo, *J. Phys. Chem. B*, 2008, **112**, 4357–4364.
- 115 J. Troncoso, C. A. Cerdeiriña, Y. A. Sanmamed, L. Romaní and L. P. N. Rebelo, *J. Chem. Eng. Data*, 2006, **51**, 1856–1859.
- 116 C. A. N. de Castro, E. Langa, A. L. Morais, M. L. M. Lopes, M. J. V. Lourenço, F. J. V. Santos, M. S. C. S. Santos, J. N. C. Lopes, H. I. M. Veiga, M. Macatrão, J. M. S. S. Esperança, C. S. Marques, L. P. N. Rebelo and C. A. M. Afonso, *Fluid Phase Equilib.*, 2010, **294**, 157–179.
- 117 K. Oster, P. Goodrich, J. Jacquemin, C. Hardacre, A. P. C. Ribeiro and A. Elsinawi, *J. Chem. Thermodyn.*, 2018, **121**, 97–111.
- 118 W. C. Barnhill, Masters Thesis, University of Tennessee, 2016.
- 119 R. González, M. Bartolomé, D. Blanco, J. L. Viesca and A. Fernández-gonzález, *Tribology Int.*, 2016, **98**, 82–93.
- 120 J. Jacquemin, P. Husson, A. A. H. Padua and V. Majer, *Green Chem.*, 2006, **8**, 172–180.
- 121 P. Bonhote, A. Dias, N. Papageorgiou, K. Kalyanasundaram and M. Gratzel, *Inorg. Chem.*, 1996, **35**, 1168–1178.
- 122 H. Tokuda, K. Hayamizu, K. Ishii, A. Hasan Susan and M. Watanabe, *J. Phys. Chem. B*, 2005, **109**, 6103–6110.
- 123 F. S. Oliveira, M. G. Freire, P. J. Carvalho, A. P. Coutinho and N. C. Lopes, *J. Chem. Eng. Data*, 2010, **55**, 4514–4520.
- 124 M. C. M. Sequeira, H. M. N. T. Avelino, F. J. P. Caetano and J. M. N. A. Fareleira, *J. Chem. Eng. Data*, 2021, **66**, 1763–1772.

- 125 J. N. C. Lopes, M. F. C. Gomes and A. A. H. Pádua, *J. Phys. Chem. B*, 2006, **110**, 16816–16818.
- 126 B. Yu, D. G. Bansal, J. Qu, X. Sun, H. Luo, S. Dai, P. J. Blau, B. G. Bunting, G. Mordukhovich and D. J. Smolenski, *Wear*, 2012, **289**, 58–64.
- 127 Y. Zhou and J. Qu, *Appl. Mater. Interfaces*, 2017, **9**, 3209–3222.
- 128 M. F. Fox and M. Priest, *Eng. Tribol.*, 2008, **222**, 291–303.
- 129 W. C. Barnhill, H. Gao, B. Kheireddin, B. L. Papke, H. Luo, B. H. West and J. Qu, *Front. Mech. Eng.*, 2015, **1**, 1–8.
- 130 M. Klimczak, P. Kern, T. Heinzelmann, M. Lucas and P. Claus, *Appl. Catal. B Environ.*, 2010, **95**, 39–47.
- 131 G. H. B. Dean, E.W. Davis, *Chem. Metall. Eng.*, 1929, **36**, 618–619.
- 132 G. W. Stachowiak and A. W. Batchelor, *Engineering Tribology*, Butterworth-Heinemann, 4th edn., 2014.
- 133 W. C. Barnhill, J. Qu, H. Luo, H. M. Meyer, C. Ma, M. Chi and B. L. Papke, .
- 134 E. K. Heikal, M. S. Elmelawy, S. A. Khalil and N. M. Elbasuny, *Egypt. J. Pet.*, 2017, **26**, 53–59.
- 135 J. Zakarian, *SAE Int. J. Fuels Lubr.*, 2012, **5**, 1123–1131.
- 136 M. Bermúdez, A. Jiménez, J. Sanes and F. Carrión, *Molecules*, 2009, **14**, 2888–2908.
- 137 C. J. Reeves, A. K. Kasar and P. L. Menezes, *J. Clean. Prod.*, 2021, **279**, Article 123666.

10. Appendix

Table 8 - Viscosity error analysis data for $[C_4(C_1Im)][NTf_2]$ where μ^a = initial viscosity and μ^b = repeated viscosity.

Temperature °C	Viscosity ^a , μ^a mPa·s	Viscosity ^b , μ^b mPa·s	Average Viscosity, μ mPa·s	Standard Deviation, σ mPa·s
20	63.02	63.41	63.21	0.19
30	41.09	41.30	41.20	0.10
40	28.33	28.48	28.40	0.07
50	20.48	20.58	20.53	0.05
60	15.40	15.47	15.44	0.04
70	11.95	12.00	11.97	0.03
80	9.52	9.57	9.54	0.03
90	7.75	7.79	7.77	0.02
100	6.44	6.46	6.45	0.01

Table 9 - Kinematic viscosity error analysis data for $[C_4(C_1Im)][NTf_2]$ where ^a = initial kinematic viscosity measurement and ^b = repeated kinematic viscosity measurement.

Temperature °C	Kinematic Viscosity ^a , ν^a mm ² /s	Kinematic Viscosity ^b , ν^b mm ² /s	Average Kinematic Viscosity, ν mm ² /s	Standard Deviation, σ mm ² /s
20	43.80	44.04	43.92	0.12
30	28.22	28.86	28.54	0.32
40	19.92	20.02	19.97	0.05
50	14.51	14.57	14.54	0.03
60	10.98	11.02	11.00	0.02
70	8.57	8.61	8.59	0.02
80	6.87	6.91	6.89	0.02
90	5.64	5.66	5.65	0.01
100	4.71	4.73	4.72	0.01

Table 10 - Density error analysis data for $[C_4(C_1Im)][NTf_2]$ where ρ^a = initial viscosity measurement and ρ^b = repeated viscosity measurement.

Temperature °C	Density ^a , ρ^a g/cm ³	Density ^b , ρ^b g/cm ³	Average Density, ρ g/cm ³	Standard Deviation, σ g/cm ³
20	1.4389	1.4398	1.4394	0.0004
30	1.4308	1.4310	1.4309	0.0001
40	1.4218	1.4226	1.4222	0.0004
50	1.4119	1.4131	1.4125	0.0006
60	1.4031	1.4038	1.4035	0.0003
70	1.3937	1.3943	1.3940	0.0003
80	1.3845	1.3852	1.3849	0.0003
90	1.3753	1.3760	1.3757	0.0003
100	1.3667	1.3669	1.3668	0.0001

Table 11 - Reversing heat capacity of a range of ILs at different temperatures.

IL	Molecular Mass	Cp(20 °C)	Cp(40 °C)	Cp(60 °C)	Cp(80 °C)	Cp(100 °C)	Cp(120 °C)
[C ₄ (C ₁ Im)][NTf ₂]	419.36	449.76 ± 0.51	459.41 ± 0.21	465.40 ± 0.17	471.81 ± 0.11	479.05 ± 0.35	486.73 ± 0.20
[C ₁₀ (C ₁ Im) ₂][NTf ₂] ₂	584.62	614.55 ± 0.35	623.62 ± 0.43	633.09 ± 0.31	641.22 ± 0.23	648.62 ± 0.62	658.23 ± 0.17
[C ₁₀ (C ₁ Pyrr) ₂][NTf ₂] ₂	590.71	745.65 ± 0.40	761.59 ± 0.47	773.72 ± 0.36	785.20 ± 0.44	800.14 ± 0.29	811.83 ± 0.28
[m-xyl-(C ₈ Im) ₂][NTf ₂] ₂	744.52	870.09 ± 0.54	892.27 ± 0.47	910.29 ± 0.46	925.59 ± 0.30	944.75 ± 0.19	962.84 ± 0.48
[N _{888H}][DEHP]	676.11	1219.08 ± 0.77	1255.76 ± 1.04	1284.09 ± 0.49	1321.50 ± 0.95	1361.52 ± 0.29	1397.98 ± 0.31
[P ₆₆₆₁₄][DEHP]	805.29	1629.51 ± 1.03	1662.13 ± 1.06	1683.07 ± 1.21	1705.87 ± 1.75	1730.54 ± 2.70	1758.56 ± 0.61

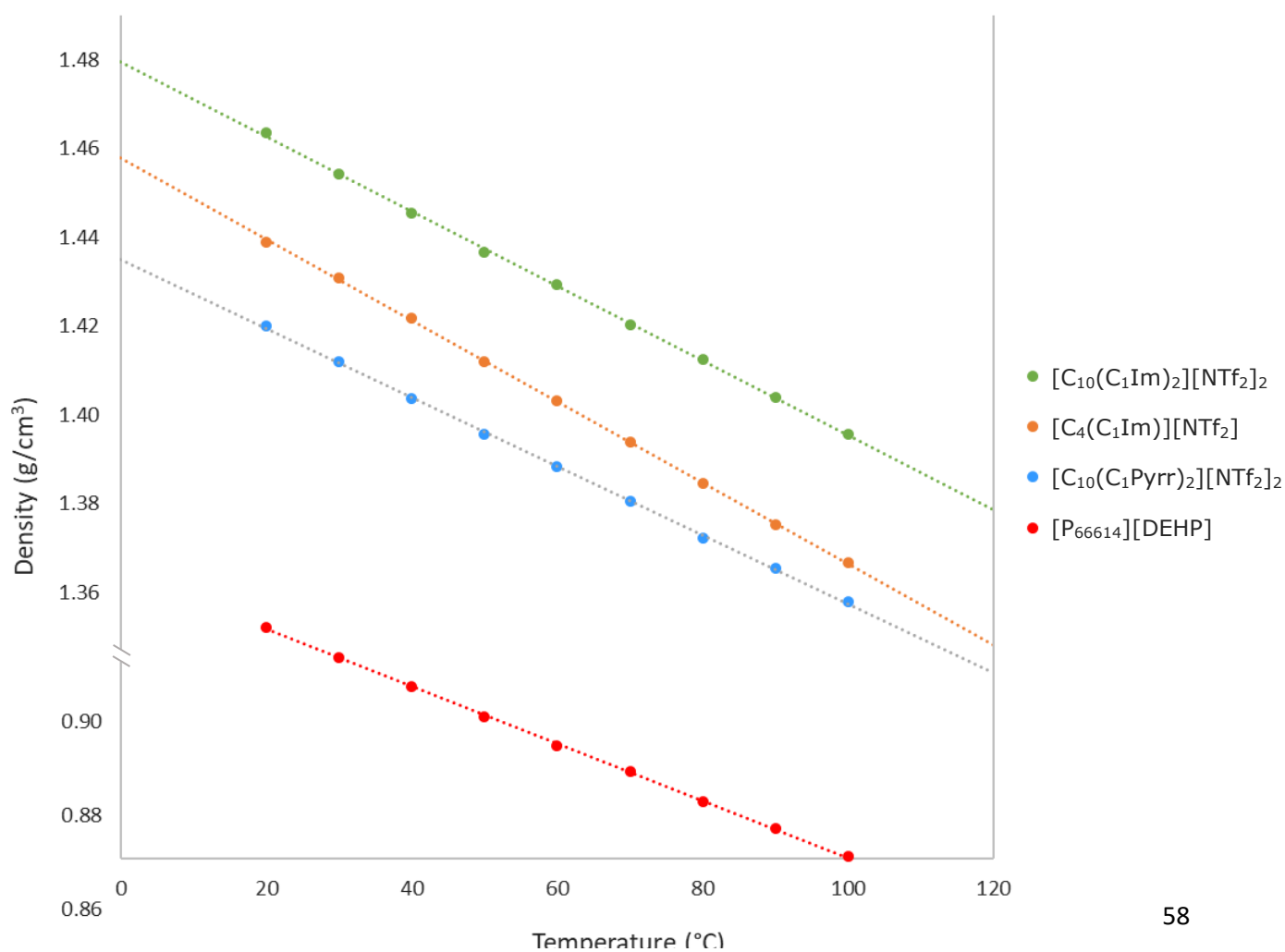


Figure 18 - Experimental densities of dried ILs.